INSTITUT DE FRANCE
Académie des sciences

Comptes Rendus
Mécanique

Abdelhak Megdoud, Belkacem Manser, Idir Belaidi, Farid Bakir and Sofiane Khelladi

A reduced-order method with PGD for the analysis of dynamically loaded journal bearing

Volume 350 (2022), p. 361-390

Published online: 20 July 2022

https://doi.org/10.5802/crmeca.124

Les Comptes Rendus. Mécanique *sont membres du Centre Mersenne pour l'édition scientifique ouverte*
www.centre-mersenne.org
e-ISSN : 1873-7234

Comptes Rendus
Mécanique
2022, Vol. 350, p. 361-390
https://doi.org/10.5802/crmeca.124

Synthesis / *Synthèse*

A reduced-order method with PGD for the analysis of dynamically loaded journal bearing

Méthode de réduction de modèle avec l'approche PGD pour l'analyse d'un palier lisse chargé dynamiquement

Abdelhak Megdoud *, [a], **Belkacem Manser** [a], **Idir Belaidi** [a], **Farid Bakir** [b] and **Sofiane Khelladi** [b]

[a] LEMI., FT., University of M'hamed Bougara, Avenue de I'indépendance, 35000-Boumerdes, Algeria

[b] Arts et Métiers Institute of Technology, CNAM, LIFSE, HESAM University, F-75013 Paris, France

E-mails: a.megdoud@univ-boumerdes.dz (A. Megdoud), b.manser@univ-boumerdes.dz (B. Manser), idir.belaidi@gmail.com (I. Belaidi), Farid.BAKIR@ensam.eu (F. Bakir), Sofiane.KHELLADI@ensam.eu (S. Khelladi)

Abstract. Machine component design has become a prominent topic for researchers in recent years. The analysis of bearing systems has received considerable attention in order to avoid detrimental contact. Among the most important studies in this area are the transient problems of journal bearings, which are usually performed by coupling the Reynolds equation with the motion equations. Many techniques have been presented in the literature and are still being explored to ensure the accurate findings and efficient solution prediction of unsteady state Reynolds equation. In this paper, the Proper Generalized Decomposition (PGD) approach is expanded for the analysis of the lubricant behavior of dynamically loaded journal bearing considering Swift-Stieber boundary conditions. The PGD model is applied in this problem, seeking the approximate solution in its separated form of the partial differential Reynolds equation at each time step during the load applied cycle employing the alternating direction strategy. Compared to the classical resolution, the PGD solution has a considerably low computational cost. To verify the accuracy and efficiency of this approach, three cases have been considered, infinitely short, infinitely long and finite journal bearings under the dynamic load. The results of the suggested methodology when compared to the full discretized model (FDM) show that, the new scheme is more efficient, converges quickly, and gives the accurate solutions with a very low CPU time consumption.

Résumé. La conception des composants de machines est devenue un sujet de premier plan pour les chercheurs ces dernières années. L'analyse des palier a fait l'objet d'une attention considérable afin d'éviter tout

* Corresponding author.

contact préjudiciable. Parmi les études les plus importantes dans ce domaine figurent les problèmes transitoires des paliers lisses, qui sont généralement réalisés en couplant les équations de Reynolds avec les équations de mouvement. De nombreuses techniques ont été présentées dans la littérature et sont encore en cours d'exploration pour garantir des résultats précis et une prédiction efficace de la solution de l'équation de Reynolds à l'état instable. Dans cet article, l'approche PGD (Proper Generalized Decomposition) est étendue pour l'analyse du comportement du lubrifiant d'un palier lisse dynamiquement chargé en considérant les conditions limites de Swift-Stieber. Le modèle PGD est appliqué à ce problème, en recherchant la solution approximative sous sa forme séparée de l'équation aux dérivées partielles de Reynolds à chaque pas de temps pendant le cycle d'application de la charge en utilisant la stratégie de direction alternée. Par rapport à la résolution classique, la solution PGD a un coût de calcul considérablement faible. Pour vérifier l'exactitude et l'efficacité de cette approche, trois cas ont été considérés, palier infiniment court, infiniment long et de longueur finie soumis à une charge dynamique. Les résultats de la méthodologie suggérée comparés au modèle discrétisé complet (FDM) montrent que le nouveau schéma est plus efficace, converge rapidement, et donne des solutions précises avec une très faible consommation du temps CPU.

Keywords. Hydrodynamic lubrication, Journal bearings, Dynamical behavior, Reynolds equation, Proper generalized decomposition, Full discretized model.

Mots-clés. Lubrification hydrodynamique, Palier lisse, Comportement dynamique, Équation de Reynolds, Décomposition propre généralisée, Modèle discrétisé complet.

Manuscript received 25 October 2021, revised 10 June 2022 and 4 July 2022, accepted 4 July 2022.

1. Introduction

Hydrodynamic bearings are critical components of rotating machines, and are widely regarded as the best technological solution currently available in a variety of industries, including thermal engines, turbo-machines, alternators, and compressors. They offer a number of benefits like high efficiency and precision, minimal friction and effective heat dissipation. The journal bearing transient analysis is frequently required in industrial applications. In engine bearings, for example, the variation of the load pressing on the bearing, and in some circumstances of the bearing's angular velocity, is so large that a static analysis is useless.

The basics of hydrodynamic lubrication was firstly established by Reynolds in 1886 [1]. Reynolds' research was influenced by prior experimental results by Petrov [2] and Tower [3], where they showed that the viscosity is the most essential characteristic in film lubrication and that the high pressures produced in the clearance space between the journal and the sleeve determine a bearing's load-carrying capacity. The so-called "Reynolds equation" which is derived from the Navier–Stokes and the continuity equations for in-compressible flows, is a second-order partial differential equation which basically predicts the pressure distribution in thin film lubrication. To solve this equation, many methods have been presented. On one hand, we have analytical models, which can produce some intriguing findings for very specific instances under certain assumptions and simplifications. We cite the following study examples: for long [4], finite [5, 6] and short [7] journal bearings. On the other hand, various numerical methods for solving fluid film lubrication problems have been established. We quote the following research examples: [8, 9] and [10] where the finite volume method has been used to solve the Reynolds equation under unsteady state conditions. In the works reported in [11] and [12] the finite element methods for the dynamically loaded journal bearing analysis was employed. Furthermore, in the studies mentioned in [13, 14] and [15] the Gauss–Siedel iterative method using the finite difference discretization was applied to treat the transient problem of journal bearing considering the Reynolds boundary conditions.

These methods are known to be accurate, but they are also very time consuming and this is not really useful for dealing with certain problems, such as, the transient hydrodynamic journal bearing problem, where, the computation procedure requires the resolution of the Reynolds equation for each time step. These issues, encourages the quest for novel procedures with

substantially reduced computational cost. Therefore, Reduced-Order Models (ROM) have been proposed to solve problems in fluid mechanics in recent decades. The most popular of these methods is an *a posteriori* method known as the Proper Orthogonal Decomposition (POD), employed by Allery *et al.* [16, 17], Atwell and King [18], Akkari *et al.* [19] and Krasnyk *et al.* [20] to solve the computational fluid problems. This category of method requires some snapshots of the flow, resulting from the higher fidelity techniques, which, necessitates a significant cost computation.

To overcome this difficulty, *a priori* techniques have been developed to find a reduced basis to describe the problem without "*a priori*" knowledge of the solution. Among these, Proper Generalized Decomposition (PGD) suggested by Ammar *et al.* [21] in 2006, which has shown to be a promising approach. The PGD is an iterative approach for decreasing the number of unknowns in a partial differential equation (PDE) by searching for the problem's solution $u(x)$ in the separating form:

$$u(x_1, x_2, \ldots, x_N) = \sum_{i=1}^{Q} \prod_{k=1}^{N} u_{ik}(x_k). \tag{1.1}$$

If M^k is the number of nodes appropriate to discretize each variable x_k, the number of unknowns will be equal to $(Q \sum_{i=1}^{N} M^k)$. Proving that for the PGD, the number of degrees of freedom evolves linearly with the number of variables. Therefore, this avoids the exponential complexity involved in traditional methods, where the number of unknowns is equal to $(\prod_{k=1}^{N} M^k)$. Moreover, for the majority of the cases, the number Q necessary for the convergence of the PGD solution is rather small (lower than ten) which considerably reduces the number of unknowns.

The PGD has been applied in various engineering problems, in biology [22] and quantum chemistry [23]. In term of fluid mechanics, the PGD was employed by Dumon *et al.* [24] to solve the Navier–Stokes equations for 2D lid-driven cavity problems. The results of this study showed that, depending on the Reynolds number, the PGD can be eight times faster than the full grid solver for standard discretization. In Aghighi *et al.* [25] papers', by applying PGD, the transient solution of non-linear coupled models linked to the Rayleigh–Bénard flow model of both Newtonian and non-Newtonian fluids is considered and the results of this study indicated that the PGD significantly reduces the computational cost. Also, another study was presented by Dumon *et al.* [26], where the PGD technique was combined with spectral discretization to solve different transfer equations. This study has shown that depending on the mesh size and the problem considered, the PGD can give results one hundred times faster for the stationary diffusion equation and ten times faster for the Navier–Stokes equations than the full model. Leblond *et al.* [27] used the PGD to build an *a priori* low-dimensional space–time separated representation of the fluid fields. In Tamellini *et al.* work's [28], the PGD was combined with stochastic Galerkin approximation and presented as a method for solving the steady incompressible Navier–Stokes equation. Le-Quoc *et al.* [29] demonstrated that the effectiveness in terms of accuracy and computational cost of the PGD which was coupled with the Immersed Boundary Method (IBM) to solve fluid-structure interaction problems taking into account the influence of complex obstacles. For hydrodynamic journal bearing analyses, Charabi *et al.* [30] used the PGD to solve the Reynolds equation in the stationary case considering Sommerfeld's and Gumbel's boundary conditions. This study showed that depending on the mesh size, the PGD is a thousand times faster than classical methods with a better convergence and less storage capacity required.

In this paper, the application of the PGD approach to the resolution of the hydrodynamic lubrication problems in journal bearings under dynamic load is considered. Furthermore, the Reynolds boundary conditions are taken into account for their good agreement with the physical reality. The dynamically loaded journal bearing analysis is realized by coupled the Reynolds and the motion equations.

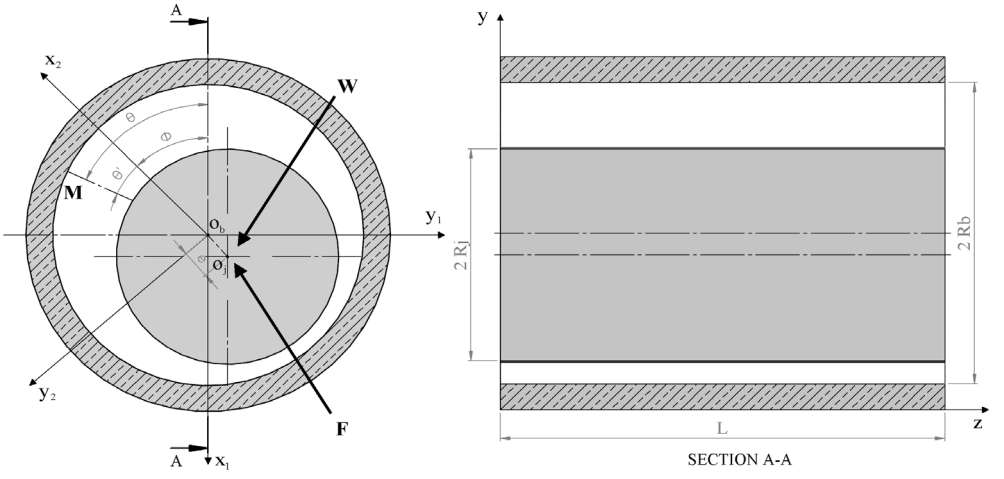

Figure 1. Coordinate system of dynamically loaded journal bearing.

The present paper is structured as follows: Section 2 describe the governing equation and the boundary condition. Section 3 is dedicated to the details of the separated representation of the unsteady state of Reynolds equation using the alternating direction strategy scheme, the computational procedure and its pseudo-code. Section 4 presents the comparison between the results obtained by the PGD and those obtained by the full discretized model using finite difference method. Finally, the report is ended with an overall conclusion and references.

2. Governing equations

2.1. *Reynolds equation*

Under simplifying assumptions [31], the Reynolds equation is employed in lubrication theory for the computation of the pressure distribution of thin viscous fluid films. It is an elliptic, partial and differential equation for the pressure in terms of lubricant properties, density and viscosity, as well as the film thickness. For a journal operating in unsteady state regime (in Cartesian coordinates), the Reynolds equation is expressed as:

$$\frac{\partial}{\partial x}\left(\frac{h^3}{12\mu}\frac{\partial P}{\partial x}\right)+\frac{\partial}{\partial z}\left(\frac{h^3}{12\mu}\frac{\partial P}{\partial z}\right)=\frac{R\omega}{2}\frac{\partial h}{\partial x}+\frac{\partial h}{\partial t} \tag{2.1}$$

where P is the pressure, h is the film thickness, R is the bearing radius, ω is the shaft's angular velocity and μ is the lubricant's viscosity.

By introducing the following dimensionless variables:

$$\theta=\frac{x}{R},\quad \overline{z}=\frac{z}{L},\quad \overline{P}=\frac{P\,c^2}{\mu R^2\omega},\quad \overline{h}=\frac{h}{c},\quad \alpha=\omega\,t,\quad \eta=\frac{D}{2L} \tag{2.2}$$

where θ is the angular position, α is the crank angle, L is the bearing length, D is the bearing diameter and c is the radial clearance.

Then the Reynolds equation with θ and $\overline{z}$ coordinates (Figure 1) becomes:

$$\frac{\partial}{\partial\theta}\left(\overline{h}^3\frac{\partial\overline{P}}{\partial\theta}\right)+\eta^2\frac{\partial}{\partial\overline{z}}\left(\overline{h}^3\frac{\partial\overline{P}}{\partial\overline{z}}\right)=6\frac{\partial\overline{h}}{\partial\theta}+12\frac{\partial\overline{h}}{\partial\alpha}. \tag{2.3}$$

The dimensionless oil film thickness is calculated from the following function:

$$\overline{h} = 1 + \varepsilon_{x1}\cos(\theta) + \varepsilon_{y1}\sin(\theta) \tag{2.4}$$

where: $\varepsilon_{x1} = e_{x1}/c$, $\varepsilon_{y1} = e_{y1}/c$ are the relatives eccentricity, e_{x1} and e_{y1} are the the eccentricity.

Considering an aligned journal bearing, the development of (2.3) gives:

$$\frac{\partial \overline{h}^3}{\partial\theta}\frac{\partial\overline{P}}{\partial\theta} + \overline{h}^3\frac{\partial^2\overline{P}}{\partial\theta^2} + \eta^2\overline{h}^3\frac{\partial^2\overline{P}}{\partial\overline{z}^2} = 6\frac{\partial\overline{h}}{\partial\theta} + 12\frac{\partial\overline{h}}{\partial\alpha} \tag{2.5}$$

and so

$$\frac{3}{\overline{h}}\frac{\partial\overline{h}}{\partial\theta}\frac{\partial\overline{P}}{\partial\theta} + \frac{\partial^2\overline{P}}{\partial\theta^2} + \eta^2\frac{\partial^2\overline{P}}{\partial\overline{z}^2} = \frac{6}{\overline{h}^3}\left(\frac{\partial\overline{h}}{\partial\theta} + 2\frac{\partial\overline{h}}{\partial\alpha}\right). \tag{2.6}$$

2.2. *Boundary conditions*

The studied bearing is with a line groove of negligible thickness, situated at $\theta = 0°$ and extending at the bearing's ends.

The boundary conditions related to the supply pressure are:

$$\overline{P}(\theta = 0, \overline{z}) = \overline{P}(\theta = 2\pi, \overline{z}) = 0 \tag{2.7}$$

$$\overline{P}(\theta, 1) = \overline{P}(\theta, 0) = 0. \tag{2.8}$$

The boundary conditions of the cavitation region are:

$$\overline{P}(\theta = \theta_1, \overline{z}) = 0 \tag{2.9}$$

$$\overline{P}(\theta = \theta_2, \overline{z}) = 0 \tag{2.10}$$

$$\frac{\partial\overline{P}}{\partial\theta}(\theta = \theta_1, \overline{z}) = 0 \tag{2.11}$$

$$\frac{\partial\overline{P}}{\partial\theta}(\theta = \theta_2, \overline{z}) = 0 \tag{2.12}$$

where θ_1 represents the location of the starting of full film zone, while θ_2 represents the location of the starting of cavitation zone.

These are the Swift-Stieber (Reynolds) boundary conditions which are applying by forcing the negative pressure to zero and forcing the pressure gradient to vanish on the frontier between the full film and the cavitation regions.

2.3. *Force balance equation*

A force balance on the journal gives:

$$\overline{W}_{x1} + \overline{F}_{x1} = \overline{M}\,\ddot{\varepsilon}_{x1} \tag{2.13}$$

and

$$\overline{W}_{y1} + \overline{F}_{y1} = \overline{M}\,\ddot{\varepsilon}_{y1} \tag{2.14}$$

where $\overline{M}$ is the dimensionless mass of the journal, the $\overline{W}_{x1}$ and $\overline{W}_{y1}$ are the components of the dimensionless externally applied load, $\overline{F}_{x1}$ and $\overline{F}_{y1}$ are the components of the dimensionless fluid film force.

where

$$\overline{F}_{x1} = \int_{\Omega_\theta\Omega_{\overline{z}}} \overline{P}\cos(\theta)\,\mathrm{d}\theta\,\mathrm{d}\overline{z} \tag{2.15}$$

$$\overline{F}_{y1} = \int_{\Omega_\theta\Omega_{\overline{z}}} \overline{P}\sin(\theta)\,\mathrm{d}\theta\,\mathrm{d}\overline{z} \tag{2.16}$$

then the total dimensionless fluid film force is given as:

$$\overline{F} = \sqrt{\overline{F}_{x1}^{2} + \overline{F}_{y1}^{2}}. \tag{2.17}$$

2.4. *Sommerfeld number*

The Sommerfeld number (S) has been useful in comparing the non-dimensional properties of different bearing arcs. The Sommerfeld number can be expressed mathematically as follows:

$$S = \frac{1}{2\pi\overline{F}}. \tag{2.18}$$

2.5. *Friction number*

The shear stress at the journal's surface is given as:

$$\tau_{xy}\,|_{y=h} = \frac{1}{2}(2y-h)\frac{\partial P}{\partial x} + \frac{\mu U}{h} \tag{2.19}$$

where U is circumferential velocity component of any arbitrary location on the journal surface.

The friction force is calculated by integrating the journal's shear stresses, its dimensionless form is given by:

$$\overline{F}_t = \int_0^1 \int_{\theta_1}^{\theta_2} A\,\mathrm{d}\theta\,\mathrm{d}\overline{z} + \int_0^1 \int_{\theta_1}^{\theta_2} A\left(\frac{\overline{h}(\theta_2)}{\overline{h}}\right)\mathrm{d}\theta\,\mathrm{d}\overline{z} \tag{2.20}$$

with

$$A = \frac{\overline{h}}{2}\frac{\partial \overline{h}}{\partial \theta} + \frac{1}{\overline{h}}(\dot{\varepsilon}_{x1}\sin(\theta) - \dot{\varepsilon}_{y1}\cos(\theta) + 1). \tag{2.21}$$

Consequently, the friction number is obtained as follows:

$$f = \frac{\overline{F}_t}{\overline{F}}. \tag{2.22}$$

2.6. *Infinitely short journal bearing (ISJB)*

In relation to the axial pressure gradient, the circumferential pressure gradient can be ignored when the ratio L/D is small. Michell [32] was the first to make this assumption, which was further established by Ocvirk and Dubois [33]. It is appropriate for bearings with an $L/D \leq 1/8$. As a result, the Reynolds equation is written as:

$$\eta^2 \overline{h}^3 \frac{\partial^2 \overline{P}}{\partial \overline{z}^2} = 6\frac{\partial \overline{h}}{\partial \theta} + 12\frac{\partial \overline{h}}{\partial \alpha} \tag{2.23}$$

applying the boundary conditions given by (2.8) and integrate the equation twice with respect to $\overline{z}$, one arrives at the following expression:

$$\overline{P} = \frac{3}{\eta^2 \overline{h}^3}\left(\frac{\partial \overline{h}}{\partial \theta} + 2\frac{\partial \overline{h}}{\partial \alpha}\right)(\overline{z}^2 - \overline{z}). \tag{2.24}$$

Detailed calculation of the positions of starting full film zone, the cavitation area and fluid film forces are mentioned in Appendix A.

2.7. *Infinitely long journal bearing (ILJB)*

In the case of an infinitely long bearing, the axial flow is ignored in comparison to the circumferential flow. For L/D ratios of up to 4, this assumption is employed. The Reynolds equation (2.5)

can thus be simplified to:

$$\frac{\partial}{\partial\theta}\left(\overline{h}^3\,\frac{\partial\overline{P}}{\partial\theta}\right)=6\,\frac{\partial\overline{h}}{\partial\theta}+12\,\frac{\partial\overline{h}}{\partial\alpha}. \tag{2.25}$$

By integrating (2.25) twice with respect to θ' and using the boundary conditions given by (2.7), (2.10) and (2.12) (see Appendix B for further derivation). The following formulation is obtained:

$$\begin{aligned}\overline{P}=\frac{3}{(1-\varepsilon^2)^2}\Bigg\{&\frac{(1-2\dot{\phi})\,\varepsilon\,(1-\varepsilon^2)^{0.5}}{1-\cos(\psi_2)}\left[2\,(\sin(\psi)-\sin(\psi_0))\,(1+\varepsilon\cos(\psi_2))\right.\\&\left.+(2\cos(\psi_2)+\varepsilon)\,(\psi_0-\psi)-\varepsilon\,(\sin(\psi)\cos(\psi)-\sin(\psi_0)\cos(\psi_0))\right]+\dot{\varepsilon}\,\frac{2\sin(\psi)}{1-\cos(\psi_2)}\\&\times\left[\frac{(2-\varepsilon\cos(\psi)-\varepsilon\cos(\psi_0))\,(\cos(\psi_0)-\cos(\psi))\,(1-\varepsilon\cos(\psi_2))}{\sin(\psi_2)}\right.\\&\left.-(2+\varepsilon^2)\,(\psi-\psi_0)+4\,\varepsilon\,(\sin(\psi)-\sin(\psi_0))-\varepsilon^2\,(\sin(\psi)\cos(\psi)-\sin(\psi_0)\cos(\psi_0))\right]\Bigg\}.\end{aligned} \tag{2.26}$$

Calculation of the positions of starting full film zone, starting of the cavitation area and fluid film forces are detailed in Appendix B.

3. PGD for the resolution of unsteady state Reynolds equation

3.1. *Separated representation related to the Reynolds equation*

The Reynolds equation (2.6) is formulated by PGD to determine different parameters, such as pressure distribution, in order to analyze the lubricating film.

In this study since the bearing is assumed to be aligned and thickness $\overline{h}$ is not a function of $\overline{z}$, so to simplify the formulations, it is assumed $(3/\overline{h})(\partial\overline{h}/\partial\theta)=A^{\theta}$ and $6/\overline{h}^3\,(\partial\overline{h}/\partial\theta+2(\partial\overline{h}/\partial\alpha))=E^{\theta}$.

For each crank angle α, the solution of the Reynolds equation (2.6) is considered in a rectangular domain $\Omega_\theta\times\Omega_{\overline{z}}=[0,2\pi]\times[0,1]$. Thus, for all suitable test functions $\overline{P}^*$, the weighted residual form of Reynolds equation is:

$$\int\limits_{\Omega_\theta\Omega_{\overline{z}}}\overline{P}^*\left[A^{\theta}\,\frac{\partial\overline{P}}{\partial\theta}+\frac{\partial^2\overline{P}}{\partial\theta^2}+\eta^2\,\frac{\partial^2\overline{P}}{\partial\overline{z}^2}\right]\mathrm{d}\theta\,\mathrm{d}\overline{z}-\int\limits_{\Omega_\theta\Omega_{\overline{z}}}\overline{P}^*\,[E^{\theta}]\mathrm{d}\theta\,\mathrm{d}\overline{z}=0. \tag{3.1}$$

Our objective is to calculate PGD approximate solution to (2.6) in the following separated form:

$$\overline{P}(\theta,\overline{z})=\sum_{i=1}^{n}X_i(\theta)\,Z_i(\overline{z}). \tag{3.2}$$

We accomplish this by computing each expansion term one at a time, enriching the PGD approximation until a satisfactory convergence criteria is met.

3.2. *Progressive construction of the separated representation*

The first $n-1$ terms are already computed of the PGD approximation, at each enrichment step $n\,(n>1)$

$$\overline{P}^{n-1}=\sum_{i=1}^{n-1}X_i\,Z_i. \tag{3.3}$$

To obtain the enriched PGD solution, we calculate the following term:

$$\overline{P}^{n}=\overline{P}^{n-1}+X_n\,Z_n=\sum_{i=1}^{n-1}X_i\,Z_i+X_n\,Z_n. \tag{3.4}$$

At the current enrichment step n, both function $X_n(\theta)$ and $Z_n(\overline{z})$ are unknown and they appear in the form of product. As a result, the problem is non-linear, and an appropriate iterative scheme is needed. The index q is used to denote a particular iteration.

$$\overline{P}^{n,q} = \overline{P}^{n-1} + X_n^q Z_n^q = \sum_{i=1}^{n-1} X_i Z_i + X_n^q Z_n^q. \tag{3.5}$$

For its simplicity, the iterative scheme of the alternating directions strategy is applied, which is calculating X_n^q from Z_n^{q-1} and then Z_n^q from X_n^q. To begin the iterative method, an arbitrary initial guess $Z_n^0(\overline{z})$ is defined. The non-linear iterations continue until a fixed point is reached within a user-defined tolerance ξ, i.e.

$$\frac{\| X_n^q Z_n^q - X_n^{q-1} Z_n^{q-1} \|_{L^2_{(\Omega)}}}{\| X_n^{q-1} Z_n^{q-1} \|_{L^2_{(\Omega)}}} < \xi. \tag{3.6}$$

If the condition (3.6) is satisfied, the following assignments will be applied $X_n \leftarrow X_n^q$ and $Z_n \leftarrow Z_n^q$. When a sufficient measure of error er_n becomes small enough $\left(er_n < \widetilde{\xi}\right)$, the enrichment process itself comes to a halt.

with:

$$er_n = \frac{\| X_n Z_n \|_{L^2_{(\Omega)}}}{\| X_1 Z_1 \|_{L^2_{(\Omega)}}}. \tag{3.7}$$

We'll go through one specific alternating direction iteration at a given enrichment step in greater detail now.

3.2.1. *Alternating direction strategy*

- Computing X_n^q from Z_n^{q-1}

In this instance, the approximation reads:

$$\overline{P}^{n,q} = \sum_{i=1}^{n-1} X_i Z_i + X_n^q Z_n^{q-1}. \tag{3.8}$$

Except for $X_n^q(\theta)$, all functions are known. For the weighted residual formulation (3.1), the simplest choice for the weight function $\overline{P}^*$ is:

$$\overline{P}^* = X_n^* Z_n^{q-1}. \tag{3.9}$$

By injecting (3.8) and (3.9) in (3.1), we get:

$$\begin{aligned} &\int_{\Omega_\theta \Omega_{\overline{z}}} X_n^* Z_n^{q-1} \left[A^\theta \frac{\partial^2 X_n^q}{\partial \theta^2} Z_n^{q-1} + \frac{\partial X_n^q}{\partial \theta} Z_n^{q-1} + \eta^2 \frac{\partial^2 Z_n^{q-1}}{\partial z^2} X_n^q \right] \mathrm{d}\theta \, \mathrm{d}\overline{z} \\ &= - \int_{\Omega_\theta \Omega_{\overline{z}}} X_n^* Z_n^{q-1} \left[\sum_{i=1}^{n-1} \left(A \frac{\partial^2 X_i}{\partial \theta^2} Z_i + \frac{\partial X_i}{\partial \theta} Z_i + \eta^2 \frac{\partial^2 Z_i}{\partial z^2} X_i \right) - E^\theta \right] \mathrm{d}\theta \, \mathrm{d}\overline{z}. \end{aligned} \tag{3.10}$$

As in the above expressions all functions of $\overline{z}$ are known, the one-dimensional integrals over $\Omega_{\overline{z}}$ can be computed as follow:

$$\begin{cases} \bar{\mu}^\theta = \displaystyle\int_{\Omega_{\overline{z}}} (Z_n^{q-1})^2 \, \mathrm{d}\overline{z} \\ \bar{\beta}^\theta = \eta^2 \displaystyle\int_{\Omega_{\overline{z}}} Z_n^{q-1} \frac{\partial^2 Z_n^{q-1}}{\partial \overline{z}^2} \, \mathrm{d}\overline{z} \\ \bar{\xi}^\theta = \displaystyle\int_{\Omega_{\overline{z}}} Z_n^{q-1} \, \mathrm{d}\overline{z} \end{cases} \quad \begin{cases} \bar{\gamma}_i^\theta = \displaystyle\int_{\Omega_{\overline{z}}} Z_n^{q-1} Z_i \, \mathrm{d}\overline{z} \\ \bar{\delta}_i^\theta = \eta^2 \displaystyle\int_{\Omega_{\overline{z}}} Z_n^{q-1} \frac{\partial^2 Z_i}{\partial z^2} \, \mathrm{d}\overline{z}. \end{cases} \tag{3.11}$$

Equation (3.10) becomes:

$$\int_{\Omega_\theta} X_n^* \left[(\bar{\mu}^\theta A^\theta) \frac{\partial^2 X_n^q}{\partial \theta^2} + (\bar{\mu}^\theta) \frac{\partial X_n^q}{\partial \theta} + (\bar{\beta}^\theta) X_n^q \right] \mathrm{d}\theta$$
$$= \int_{\Omega_\theta} X_n^* \left(- \sum_{i=1}^{n-1} \left[(\bar{\gamma}_i^\theta A^\theta) \frac{\partial^2 X_i}{\partial \theta^2} + (\bar{\gamma}_i^\theta) \frac{\partial X_i}{\partial \theta} + (\bar{\delta}_i^\theta) X_i \right] + (\xi^\theta E^\theta) \right) \mathrm{d}\theta. \tag{3.12}$$

Thus, we have obtained the weighted residual form of a one-dimensional problem defined over Ω_θ, which can be solved (e.g., using the finite element method) to obtain the function X_n^q.

Alternatively, it can also return to the corresponding strong formulation as follow:

$$\bar{\mu}^\theta A^\theta \frac{\partial^2 X_n^q}{\partial \theta^2} + \bar{\mu}^\theta \frac{\partial X_n^q}{\partial \theta} + \bar{\beta}^\theta X_n^q = - \sum_{i=1}^{n-1} \left[\bar{\gamma}_i^\theta A^\theta \frac{\partial^2 X_i}{\partial \theta^2} + \bar{\gamma}_i^\theta \frac{\partial X_i}{\partial \theta} + \bar{\delta}_i^\theta X_i \right] + \xi^\theta E^\theta. \tag{3.13}$$

The strong form (3.13) is a second order ordinary differential equation for X_n^q. We can solve it numerically using any appropriate numerical method (for example, finite differences, pseudo-spectral techniques, etc.).

To adapt the PGD to the supply pressure boundary condition, the following changes should be made:

$$X_n^q(\theta = 0) = X_n^q(\theta = 2\pi) = 0. \tag{3.14}$$

Moreover, for the Reynolds boundary conditions, during the calculation of $X_n^q(\theta)$, the pressure must be positive. Then the following condition is defined as:

$$\overline{P}^{n-1}(\theta, \overline{z}) + X_n^q(\theta) Z_n^{q-1}(\overline{z}) \geq 0. \tag{3.15}$$

If not, then the following change will be applied $X_n^q \leftarrow -\overline{P}^{n-1} / Z_n^{q-1}$ to vanish the negative pressure.

After computing X_n^q. We are now able to proceed on to the second step of iteration q.

- Computing Z_n^q from X_n^q

The technique is identical to what we did previously. Indeed, we simply switch the roles of all related θ and $\overline{z}$ functions.

In this case, the approximation reads:

$$\overline{P}^{n,q} = \sum_{i=1}^{n-1} X_i Z_i + X_n^q Z_n^q. \tag{3.16}$$

Where all functions are known except $Z_n^q(\overline{z})$.

The simplest choice for the weight function $\overline{P}^*$ is:

$$\overline{P}^* = Z_n^* X_n^q. \tag{3.17}$$

By introducing (3.16) and (3.17) in (3.1), we obtain:

$$\int_{\Omega_\theta \Omega_{\overline{z}}} Z_n^* X_n^q \left[A^\theta \frac{\partial^2 X_n^q}{\partial \theta^2} Z_n^q + \frac{\partial X_n^q}{\partial \theta} Z_n^q + \eta^2 \frac{\partial^2 Z_n^q}{\partial z^2} X_n^q \right] \mathrm{d}\theta \, \mathrm{d}\overline{z}$$
$$- \int_{\Omega_\theta \Omega_{\overline{z}}} Z_n^* X_n^q \left(\sum_{i=1}^{n-1} \left[A^\theta \frac{\partial^2 X_i}{\partial \theta^2} Z_i + \frac{\partial X_i}{\partial \theta} Z_i + \eta^2 \frac{\partial^2 Z_i}{\partial z^2} X_i \right] + E^\theta \right) \mathrm{d}\theta \, \mathrm{d}\overline{z}. \tag{3.18}$$

Since all functions of θ are known, we can compute the integrals over Ω_θ to obtain the following expressions:

$$\begin{cases} \bar{\mu}^{\overline{z}} = \eta^2 \int\limits_{\Omega_\theta} \left(X_n^q\right)^2 \mathrm{d}\theta \\ \bar{\beta}^{\overline{z}} = \int\limits_{\Omega_\theta} X_n^q \dfrac{\partial^2 X_n^q}{\partial\theta^2} A^\theta \mathrm{d}\theta \\ \eta^{\overline{z}} = \int\limits_{\Omega_\theta} X_n^q \dfrac{\partial X_n^q}{\partial\theta} \mathrm{d}\theta \\ \xi^{\overline{z}} = \int\limits_{\Omega_\theta} X_n^q E^\theta \mathrm{d}\theta \end{cases} \quad \begin{cases} \bar{\gamma}_i^{\overline{z}} = \eta^2 \int\limits_{\Omega_\theta} X_n^q X_i \mathrm{d}\theta \\ \bar{\delta}_i^{\overline{z}} = \int\limits_{\Omega_\theta} X_n^q \dfrac{\partial^2 X_i}{\partial\theta^2} A^\theta \mathrm{d}\theta \\ \vartheta_i^{\overline{z}} = \int\limits_{\Omega_\theta} X_n^q \dfrac{\partial X_i}{\partial\theta} \mathrm{d}\theta. \end{cases} \tag{3.19}$$

Equation (3.18) reduces to:

$$\int\limits_{\Omega_{\overline{z}}} Z_n^* \left((\bar{\beta}^{\overline{z}}) Z_n^q + (\bar{\mu}^{\overline{z}}) \frac{\partial^2 Z_n^q}{\partial \overline{z}^2} + (\bar{\eta}^{\overline{z}}) Z_n^q \right) \mathrm{d}\overline{z}$$

$$= \int\limits_{\Omega_{\overline{z}}} Z_n^* \left(- \sum_{i=1}^{n-1} \left[(\bar{\delta}_i^{\overline{z}}) Z_i + (\vartheta_i^{\overline{z}}) Z_i + (\bar{\gamma}_i^{\overline{z}}) \frac{\partial^2 Z_i}{\partial \overline{z}^2} \right] + (\xi^{\overline{z}}) \right) \mathrm{d}\overline{z}. \tag{3.20}$$

As previously, the weighted residual form of an elliptic problem defined over $\Omega_{\overline{z}}$ whose solution is the function Z_n^q has been obtained. The strong formulation of this one-dimensional problem is as follows:

$$\bar{\beta}^{\overline{z}} Z_n^q + \bar{\mu}^{\overline{z}} \frac{\partial^2 Z_n^q}{\partial \overline{z}^2} + \bar{\eta}^{\overline{z}} Z_n^q = - \sum_{i=1}^{n-1} \left[\bar{\delta}_i^{\overline{z}} Z_i + \vartheta_i^{\overline{z}} Z_i + \bar{\gamma}_i^{\overline{z}} \frac{\partial^2 Z_i}{\partial \overline{z}^2} \right] + \xi^{\overline{z}}. \tag{3.21}$$

To adapt the PGD to the supply pressure boundary condition, the following changes should be applied:

$$Z_n^q(\overline{z} = 0) = Z_n^q(\overline{z} = 1) = 0. \tag{3.22}$$

Also, for the Reynolds boundary conditions, during the calculation of Z_n^q, the pressure should remain positive:

$$\overline{P}^{n-1} + X_n^q Z_n^q \geq 0 \tag{3.23}$$

if this condition (3.23) is not satisfied, then $Z_n^q \leftarrow -\overline{P}^{n-1} / X_n^q$.

3.3. *Computational procedure*

The steps for determining the characteristics of journal bearing under a dynamic cyclic load are as follows. First, arbitrary position and the velocity components of journal center (ε_{x1}^0, ε_{y1}^0, $\dot{\varepsilon}_{x1}^0$, $\dot{\varepsilon}_{y1}^0$) at the initial crank angle (α^0) are proposed. Then, the oil film pressure at this crank angle is calculated by solving the modified Reynolds (2.6). After that, the related oil film force can be immediately obtained using (2.15) and (2.16). Next the position and velocity components (ε_{x1}^1, ε_{y1}^1, $\dot{\varepsilon}_{x1}^1$, $\dot{\varepsilon}_{y1}^1$) of the journal center at the next crank angle (α^1), are obtained by solving (2.13) and (2.14) simultaneously, using the Runge–Kutta 4th order method. It should be emphasized that, for better convergence of the solution, a tolerance for the adjacent eccentricity ratio is specified as follows:

$$\varepsilon_{x1}^{k+1} - \varepsilon_{x1}^k \leq 0.001 \quad \text{and} \quad \varepsilon_{y1}^{k+1} - \varepsilon_{y1}^k \leq 0.001. \tag{3.24}$$

If these conditions are not verified, the crank angle step should be taken as $\Delta\alpha/2$ till the (3.24) is satisfied. Another tolerance for the periodic condition is defined by the following:

$$\varepsilon_{x1}^n - \varepsilon_{x1}^0 \leq 0.005 \quad \text{and} \quad \varepsilon_{y1}^n - \varepsilon_{y1}^0 \leq 0.005. \tag{3.25}$$

When the conditions above (3.25) are simultaneously satisfied, the iterative procedure method is stooped. Otherwise, the initials positions are replaced by the finales positions $(\varepsilon_{x1}^{n}, \varepsilon_{y1}^{n})$, and all of the journal center positions and velocities over a load cycle have to be re-determined again.

3.3.1. *PGD program description*

Algorithm 1 describes the Matlab implementation of the PGD source code. The steps are as follows:

(1) The bearing characteristic, the load applied and the meshing parameters are defined.
(2) The initial conditions and the step along the direction of the crank angle are determined by the procedure explained above.
(3) The Reynolds equation is solved at each crank angle by the PGD from two loops: the main enrichment operation is carried out in the outer loop, which ends when the criteria (3.7) is satisfied. The non-linear iterations in the inner loop continue until a fixed point is reached within the tolerance given in (3.6), the entire process is explained in 3.2.1.
(4) The resolution of motion equation gives the parameters needed to solve the Reynolds equation for the next crank angle.
(5) The Sommerfeld and number of friction numbers are computed at the end of the procedure.

Algorithm 1: Pseudo-code of the implemented PGD approach

1:Impute data (bearing characteristics, dynamic load, meshing parameters for N_α , N_θ and $N_{\overline{z}}$, $\tilde{\xi}$, ξ,maximum number of enrichment($\text{Max}_{\text{terms}}$), maximum number of iterations in the fixed point loop (Max_{fp}) and arbitrary initials conditions
2:**while** ((3.25) is not satisfied) **do** (the loop of research of the initial conditions)
3: **for** $k = 1 : N_\alpha$ **do** (Compute the pressure field for α_k)
4: **for** i=1 : $\text{Max}_{\text{terms}}$ **do** (main enrichment loop)
5: Initialization of the fixed point loop:
$X(\theta)$=random($N\theta$, 1), $Z(\overline{z})$=random(Nz, 1)
6: Definition of the boundary conditions to the supply pressure
7: **for** j=1:Max_{fp} **do** (main enrichment loop)
8: Save the old values of X(θ) and Z($\overline{z}$)
9: Procedure Alternating Direction Strategy
10: Compute X(θ)by Resolution of the (3.13)
11: Compute Z($\overline{z}$)by Resolution of the (3.21)
12: Compute er_p(3.6)
13: **if** $er_p < \xi$ **then**
14: Break (stopping from fixed point iterations)
15: Compute er_n (3.7)
16: **if** $er_n < \tilde{\xi}$ **then**
17: Break (stopping from the main enrichment loop)
18: Compute the fluid film force ((2.15) and (2.16))
19: Resolution of motion equation
20: If (the conditions (3.24)is not satisfied) **then** ($N_\alpha = N_\alpha \times 2$, $K = 1$)

Table 1. Infinitely short journal bearing characteristics

Parameters	Infinitely short journal bearing	Infinitely long journal bearing
Bearing length, L (m)	6×10^{-3}	300×10^{-3}
Bearing radius, R (m)	25×10^{-3}	15×10^{-3}
Relative clearance, c (m)	3.6×10^{-5}	3.6×10^{-4}
Rotational speed, N (rpm)	5000	5000
Lubricant viscosity, μ (Pa·s)	8.1×10^{-2}	8.1×10^{-2}
Mass of journal, M (kg)	306.7	3313.4
Grids, $N_\alpha\, N_\theta\, N_{\bar{z}}$	$1000 \times 81 \times 509$	$1000 \times 81 \times 509$

4. Numerical results and discussions

In this section, to examine the accuracy and the efficiency of PGD method for solving the unsteady state Reynolds equation considering the Swift-Steiber boundary conditions, two cases are considered. In the first one, a comparison of the computed fluid film pressure obtained by the PGD, the full discretized model (FDM) and the analytical solution, for an infinitely short journal bearing (ISJB), under dynamic load, is presented. This comparison is expanded to include the journal center orbit, Sommerfeld and friction numbers. After that, another comparison is also made in terms of computational cost of each numerical method mentioned above. In the second case, the same comparisons between the results obtained from the PGD and the full discretization model are carried out for the dynamic loaded finite journal bearing (FJB).

The PGD related parameters for the following study have been chosen as follows:

- Termination criterion used for the fixed point iterations: $\xi = 10^{-8}$
- Termination criterion employed for the enrichment process: $\widetilde{\xi} = 10^{-5}$
- Maximum number of enrichment: $\text{Max}_{\text{terms}} = 4$
- Maximum number of iterations in the fixed point loop: $\text{Max}_{\text{fp}} = 20$.

For the Full discretized model, the finite differences method is used with the central difference scheme of spacial discretization, the Gauss–Seidel's iterative process is employed to solve the resulting linear system, with successive over-relaxation (SOR), where $\Omega_{\text{SOR}} = 1.8$, to accelerate the convergence process.

Note that, number of nodes in the crank angle direction ($N_t = 1000$) verifies the conditions (3.24) for all node configurations.

The parameter chosen to study the convergence of the mesh, is the Sommerfeld number which depends directly on the integral of the pressure field.

The relative error related to this parameter, for a given mesh, is:

$$E_S(i) = \frac{\|S^i - S^{i-1}\|_{L^2(\alpha)}}{\|S^{i-1}\|_{L^2(\alpha)}} \tag{4.1}$$

where S^i is the vector of the Sommerfeld number computed for a given set of nodes ($N_\alpha^i \times N_\theta^i \times N_{\bar{z}}^i$).

4.1. *Infinitely short and long journal bearings*

The parameters associated with this study are described in Table 1 and the dynamic load the applied load is plotted in Figure 2.

In this section, the results obtained from the PGD, FDM and analytical solutions are compared in terms of: pressure distributions, journal center orbits, Sommerfeld and friction numbers, mesh convergence and computational time.

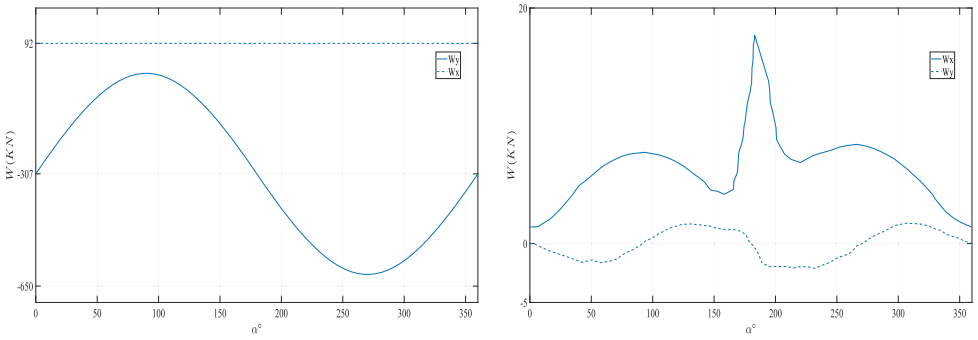

(a) The load applied on the bearing Infinitely short journal bearing

(b) The load applied on the bearing Infinitely long journal bearing

Figure 2. The applied load as a function of crank angle.

4.1.1. *Pressure distributions*

The pressure distributions obtained by PGD, analytic and FDM solutions, at $\alpha = 180°$ and $\alpha = 270°$, are illustrated in Figures 3, 4 and Figures 5, 6, respectively. While, Figures 7, 8 and 9 present the pressure distributions along the circumferential direction, at $\overline{z} = 0, \overline{z} = 0.5$ and $\overline{z} = 0.75$, for different dimensionless time values ($\alpha = 54°$, $\alpha = 180°$ and $\alpha = 270°$, respectively).

We notice that the pressure curves provided by all the approaches are quite close. Moreover, the solutions obtained from the PGD and the FDM are closer to each other than the analytical solution. This can be explained by the fact that, for the analytical solution, the pressure variation along the circumferential direction for the infinitely short journal bearing and along the axial direction for the infinitely long journal bearing are neglected. Also, through these curves it can be seen that the PGD solver yields practically the same angles of rupture of the fluid film related to Swift-Steiber boundary conditions as those provided by the FDM.

These comparison tests are insufficient to assess the pressure computation accuracy throughout the entire domain. For a more complete comparison, the evaluation of the journal center orbits and the assessment of the Sommerfeld and friction numbers are done in the next subsections.

4.1.2. *Journal center orbits*

Figure 10 shows the comparison of journal center orbits determined by the PGD, FDM and analytic solutions. It can be observed from this figure that, the trajectories of all methods have the same shape and are relatively near. However, the orbits estimated by numerical methods (PGD and FDM) are the closest to each other.

4.1.3. *Sommerfeld and friction numbers*

Figures 11 and 12 illustrate the comparison of Sommerfeld and friction numbers as a function of crank angle calculated by the PGD, FDM and analytic solutions. It is noted that all performances calculated with the proposed method (PGD) agrees with those obtained by other approaches. Furthermore, as for the previous findings, the results obtained by the PGD and the FDM are the closest between them. For a more accurate comparison, a mesh convergence study is described in next sub-section.

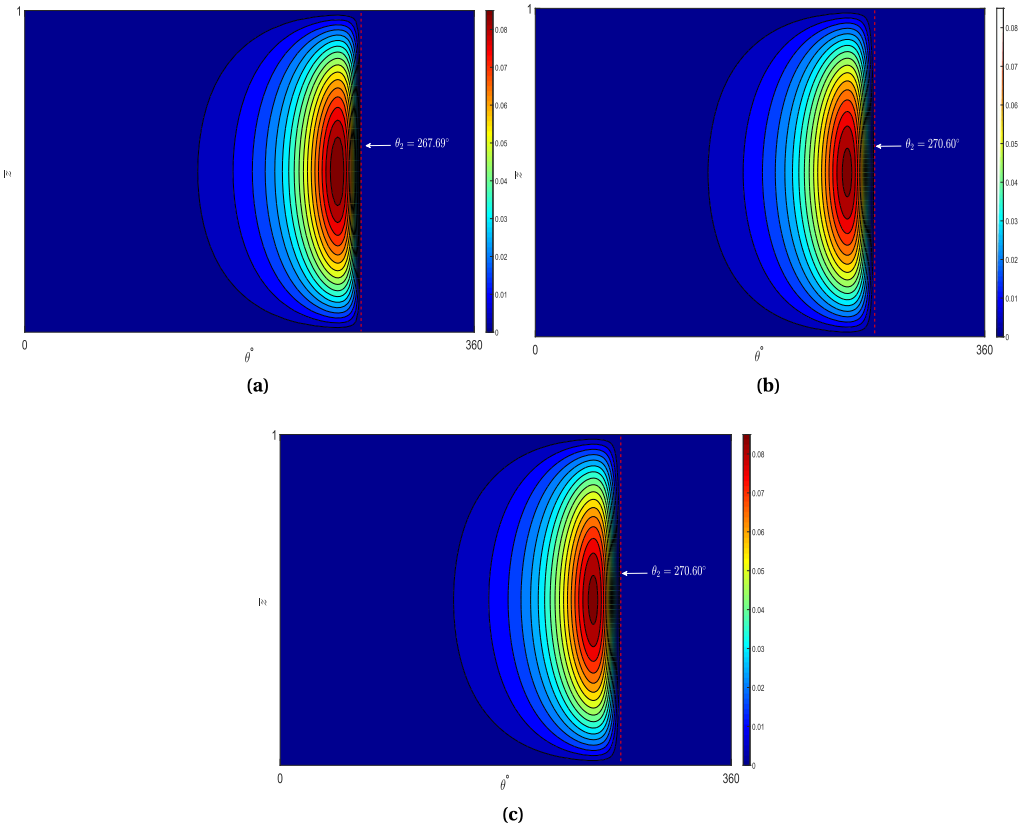

Figure 3. Dimensionless pressure distribution versus axial and circumferential coordinates at $\alpha = 180°$ obtained by: (a) analytic solution; (b) PGD and (c) FDM for ISJB.

Table 2. Error in Sommerfeld number computation for ISJB using PGD and FDM

Mesh	Error E_S for ISJB		Error E_S for IlJB	
	PGD	FDM	PGD	FDM
$1000 \times 41 \times 295$	8.2903×10^{-5}	1.5127×10^{-4}	0.0045	0.0159
$1000 \times 51 \times 321$	4.8568×10^{-5}	7.9887×10^{-5}	0.0026	0.0110
$1000 \times 61 \times 383$	3.2599×10^{-5}	7.3168×10^{-5}	0.0018	0.0094
$1000 \times 71 \times 447$	2.4667×10^{-5}	6.8958×10^{-5}	0.0012	0.0028
$1000 \times 81 \times 509$	1.7058×10^{-5}	6.3425×10^{-5}	0.0010	0.0026
$1000 \times 91 \times 573$	1.4544×10^{-5}	6.3425×10^{-5}	0.0007	0.0016
$1000 \times 101 \times 653$	1.0902×10^{-5}	6.0669×10^{-5}	0.0006	0.0015

4.1.4. *Mesh convergence study*

The convergence study is established using different sets of meshes. The results obtained by the PGD and the FDM are listed in Table 2 and plotted in Figure 13.

From the comparison, it can be observed that the convergence rate of the PGD is relatively better than that of the FDM. However, a finer mesh yields a more accurate results. The computation time rises as the mesh becomes finer. As a result, a study of the computational time needed for the PGD resolution method is more than necessary.

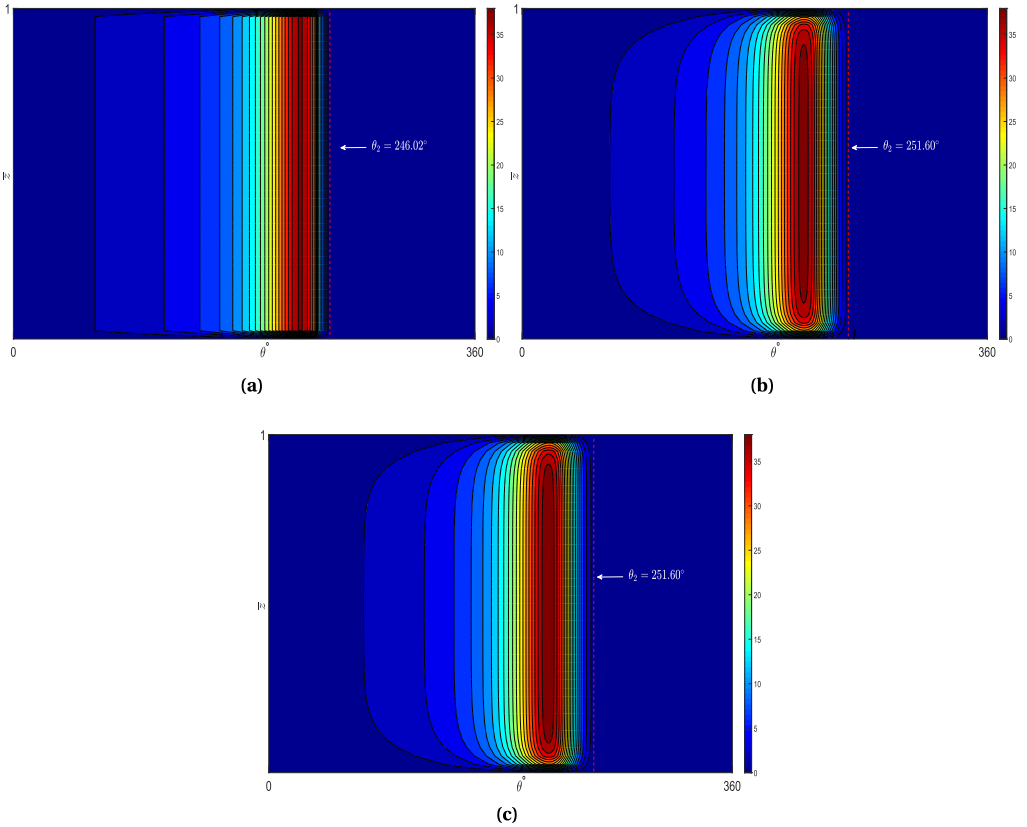

Figure 4. Dimensionless pressure distribution versus axial and circumferential coordinates at $\alpha = 180°$ obtained by: (a) analytic solution; (b) PGD and (c) FDM for ILJB.

Table 3. PGD versus FDM, computational time for different mesh numbers

Mesh	Computational time for ISJB		Computational time for ILJB	
	PGD	FDM	PGD	FDM
$1000 \times 31 \times 195$	77.45	534.96	365	4157
$1000 \times 41 \times 295$	80.69	1757.01	703	10,860
$1000 \times 51 \times 321$	119.24	4208.71	707	21,201
$1000 \times 61 \times 383$	238.72	8884.54	726	43,148
$1000 \times 71 \times 447$	281.45	16532.74	815	71,432
$1000 \times 81 \times 509$	362.42	27376.21	1387	95,029
$1000 \times 91 \times 573$	473.52	43541.36	1551	138,131
$1000 \times 101 \times 635$	655.68	66008.14	1779	189,562

4.1.5. *Computational time*

The computational time required to calculate the pressure fields as a function of mesh numbers using PGD and FDM is represented in Table 3 and Figure 14. Note that, the computational time are performed on Intel Core i7-7820HQ CPU @ 2.90 GHz (48 GB RAM, 64 bit) using Matlab.

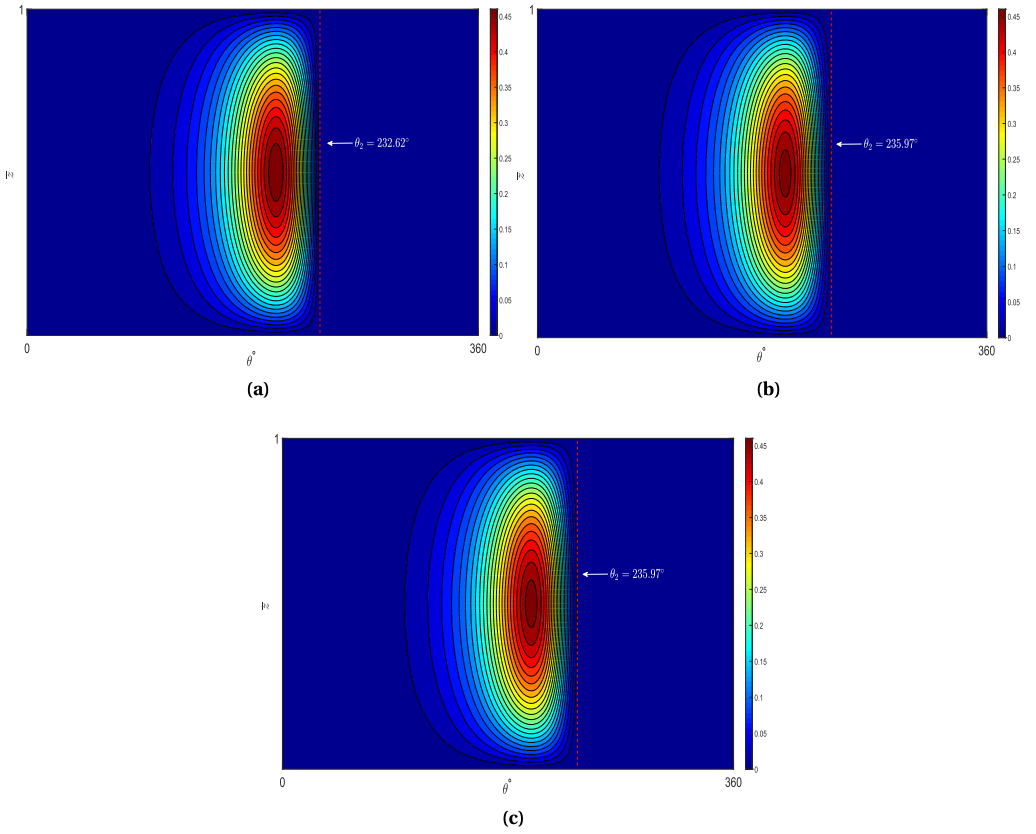

Figure 5. Dimensionless pressure distribution versus axial and circumferential coordinates at $\alpha = 270°$ obtained by: (a) analytic solution; (b) PGD and (c) FDM for ISJB.

The efficiency of PGD as compared to FDM in terms of computational time is evident from this comparison (Table 3 and Figure 14). We've seen that, in comparison to FDM, the PGD takes a lot less time as the mesh gets finer. For example, for a mesh size of $1000 \times 101 \times 635$ the PGD is more hundred times faster than the FDM. This can be justified by the fact that solving systems of linear equations consumes the majority of the CPU time required by each numerical approach (PGD and FDM). In case of the PGD, the resulting linear systems are solving by LU factorization with partial pivoting. A square matrix of N order requires $[(2/3)\,N^3]$ floating-point arithmetic operations (flops) to factorize into L and U. Then, to solve the problem of journal bearings under dynamic loading with a mesh of size $N_t\,N_\theta\,N_{\overline{z}}$, the maximum number of flops needed for the linear systems resulting by the PGD is equal to $[N_t\,(2/3)\,(N_\theta^3 + N_{\overline{z}}^3)\,\mathrm{Max_{terms}Max_{fp}}]$. In our case, maximum number of flops is equal to $[1000\,((2/3)\,\times\,N_\theta^3 + (2/3)\,N_{\overline{z}}^3)\,4\,20]$. However, to solve the same size of the problem $(N_t\,N_\theta\,N_{\overline{z}})$ by the full discretization model (FDM), using the Gauss–Siedel method, is more expensive in terms of CPU time than using LU factorization, which needs $[N_t\,(2/3)\,N_\theta^3\,N_{\overline{z}}^3]$ flops to solve linear system.

4.2. *Finite journal bearing*

The dynamically loaded finite journal bearing (FJB) analysis can be used to conduct a more global examination of the suggested method's capabilities.

The parameters of a typical automotive crankshaft bearing and the applied load cycle are taken from Wang *et al.* paper's [15] and described in Table 4 and Figure 15.

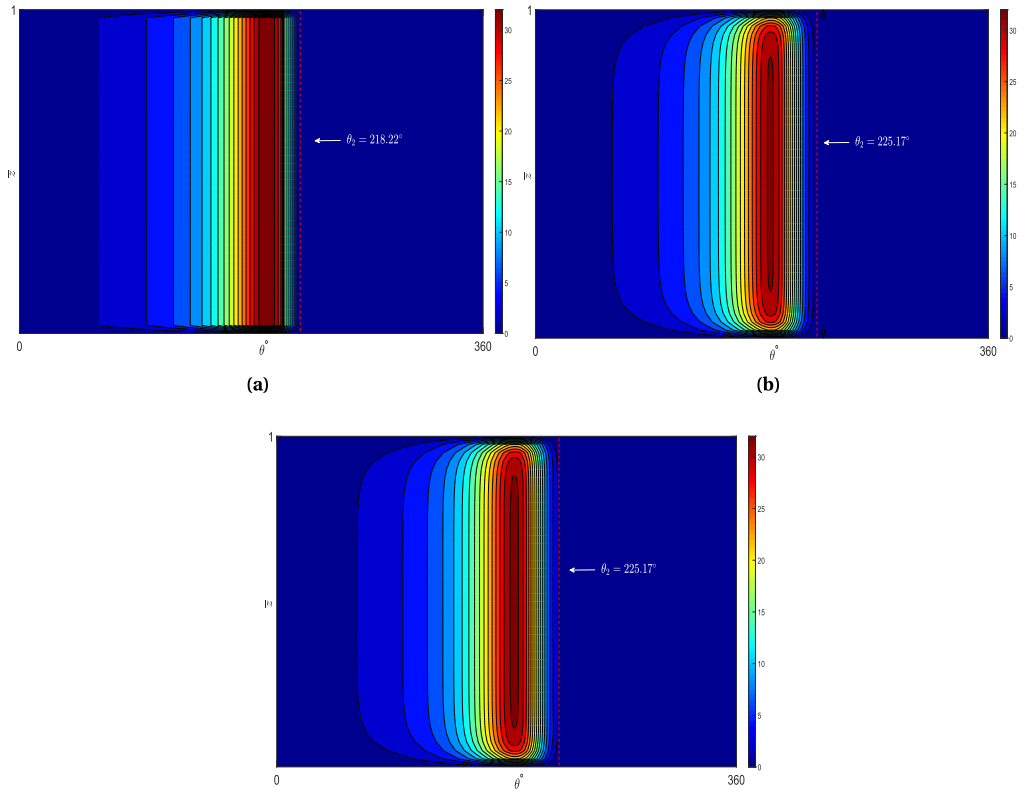

Figure 6. Dimensionless pressure distribution versus axial and circumferential coordinates at $\alpha = 270°$ obtained by: (a) analytic solution; (b) PGD and (c) FDM for ILJB.

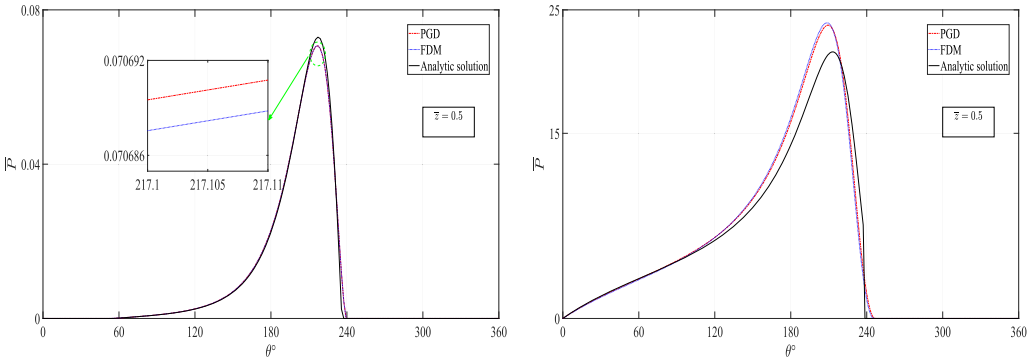

(a) The pressure distribution for ISJB

(b) The pressure distribution for ILJB

Figure 7. Pressure curves along the circumferential direction at mid-line ($\overline{z} = 0.5$) for $\alpha = 56°$.

In this section, the results obtained from the PGD and FDM predictions are also compared in terms of: pressure distributions, journal center orbits, Sommerfeld and friction numbers, mesh convergence and the computational time.

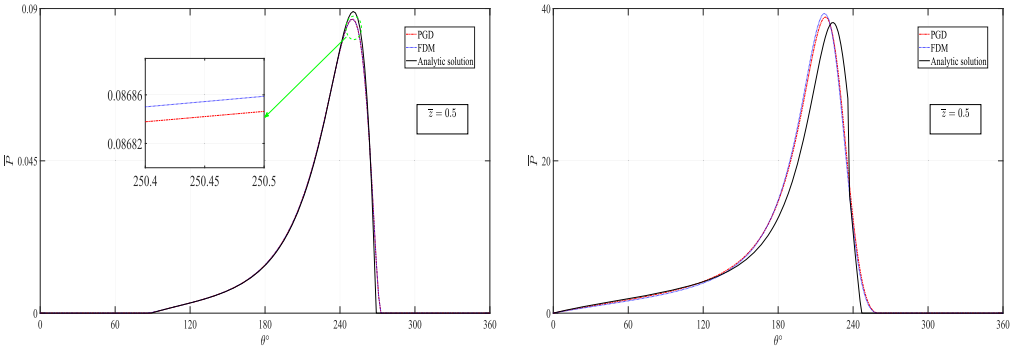

(a) The pressure distribution for ISJB **(b)** The pressure distribution for ILJB

Figure 8. Pressure curves along the circumferential direction at mid-line ($\overline{z} = 0.5$) for $\alpha = 180°$.

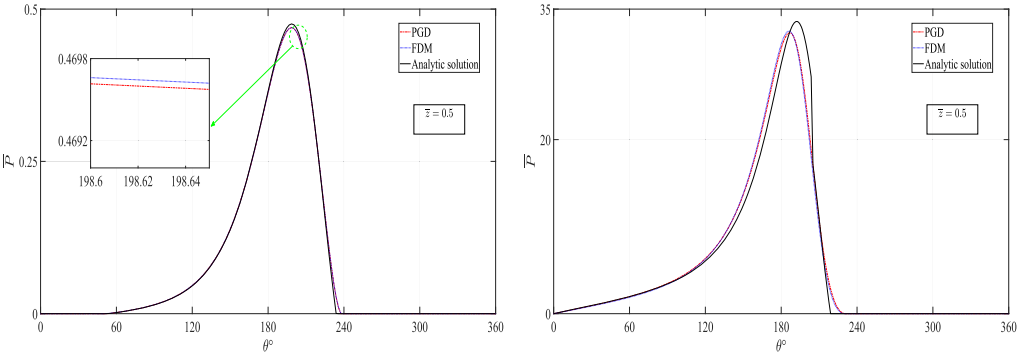

(a) The pressure distribution for ISJB **(b)** The pressure distribution for ILJB

Figure 9. Pressure curves along the circumferential direction at mid-line ($\overline{z} = 0.5$) for $\alpha = 270°$.

Table 4. Finite journal bearing characteristics [15]

Bearing length, L (m)	21×10^{-3}
Bearing radius, R (m)	36×10^{-3}
Relative clearance, c (m)	3.6×10^{-5}
Rotational speed, N (rpm)	5000
Lubricant viscosity, μ (Pa·s)	8.1×10^{-2}
Mass of journal, M (kg)	3206.3
Grids, $N_\alpha\ N_\theta\ N_{\bar{z}}$	$1000 \times 81 \times 509$

4.2.1. *Pressure distributions*

Figures 16 and 17 show the pressure fields generated by PGD and FDM procedures at $\alpha = 180°$ and $\alpha = 270°$. While, Figures 18, 19 and 20 represent the pressure distribution along the circumferential direction at mid-line ($\overline{z} = 0.5$), for different crank angles ($\alpha = 54°$, $\alpha = 180°$ and $\alpha = 270°$), where the load intensities are $W = 34{,}938$ kN, $W = 15{,}133$ kN and $W = 30{,}067$ kN respectively.

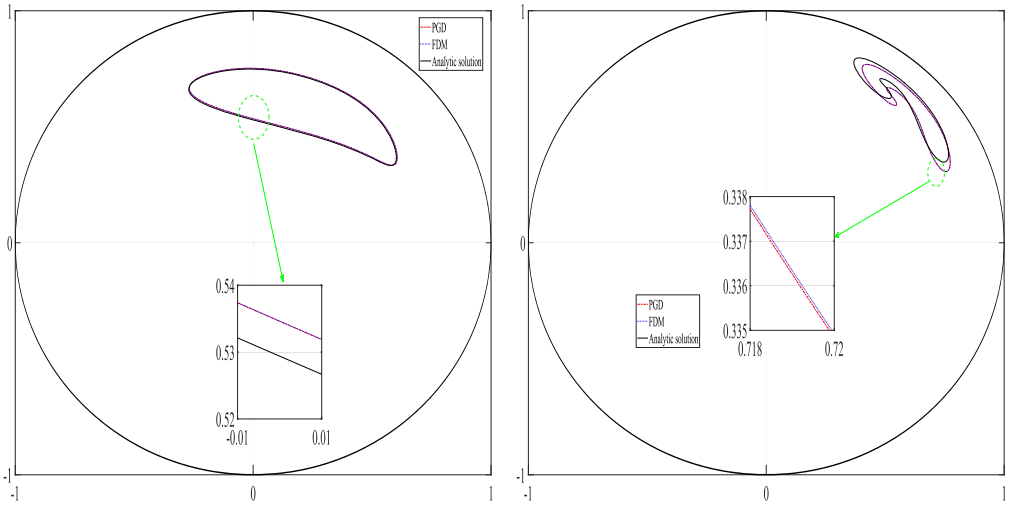

(a) Trajectory obtained for ISJB **(b)** Trajectory obtained for ILJB

Figure 10. Journal center orbit over a load cycle.

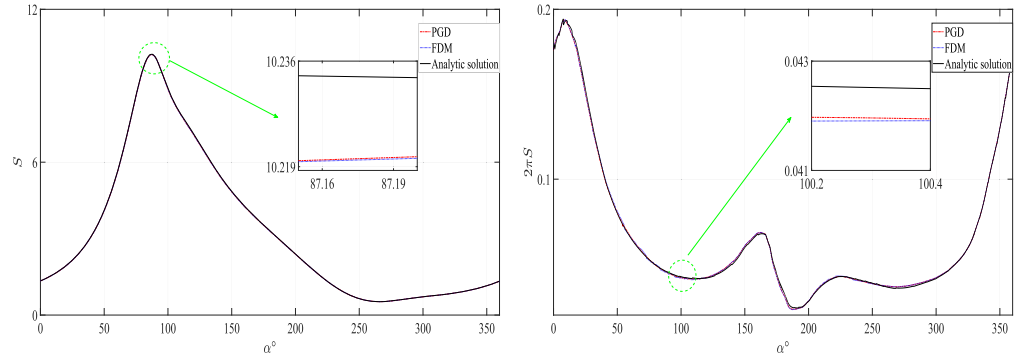

(a) The Sommerfeld number Obtained for the ISJB **(b)** The Sommerfeld number Obtained for the ILJB

Figure 11. Variation of Sommerfeld number as a function of the crank angle.

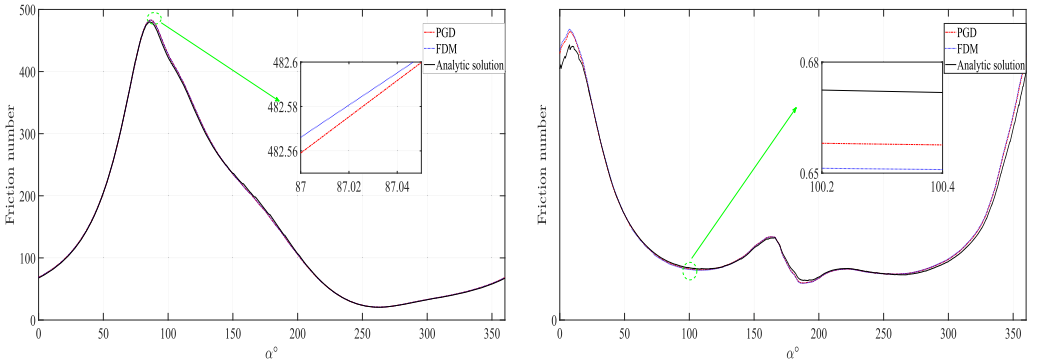

(a) The friction number obtained by ISJB **(b)** The friction number obtained by ILJB

Figure 12. Variation of friction number as a function of the crank angle.

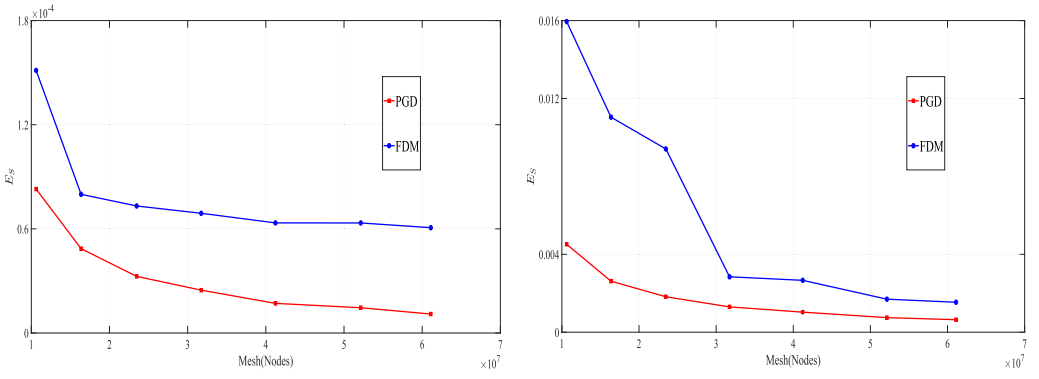

(a) Error obtained by ISJB **(b)** Error obtained by ILJB

Figure 13. Error in Sommerfeld number computation for ISJB using PGD and FDM.

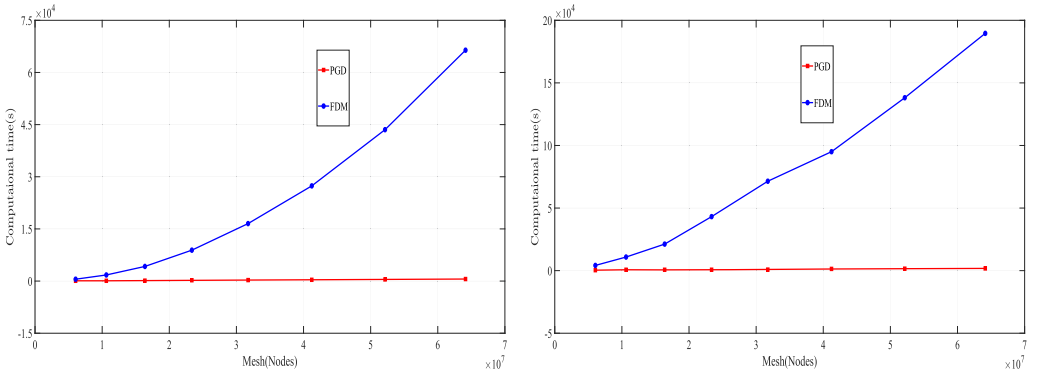

(a) Computational time consumed by ISJB **(b)** Computational time consumed by ILJB

Figure 14. PGD versus FDM computational time for different mesh numbers.

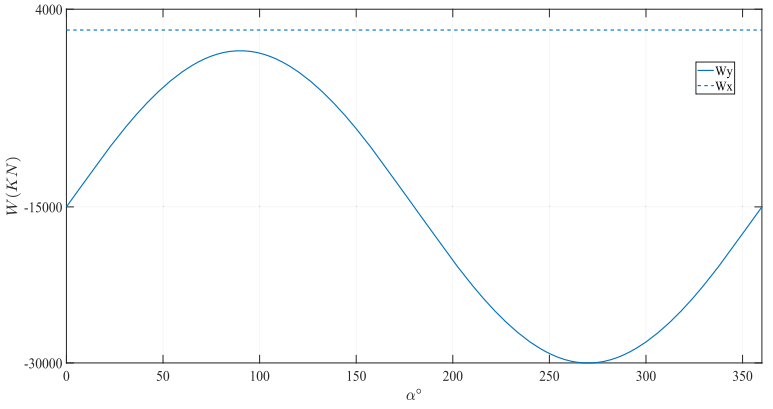

Figure 15. Applied load as a function of crank angle [15].

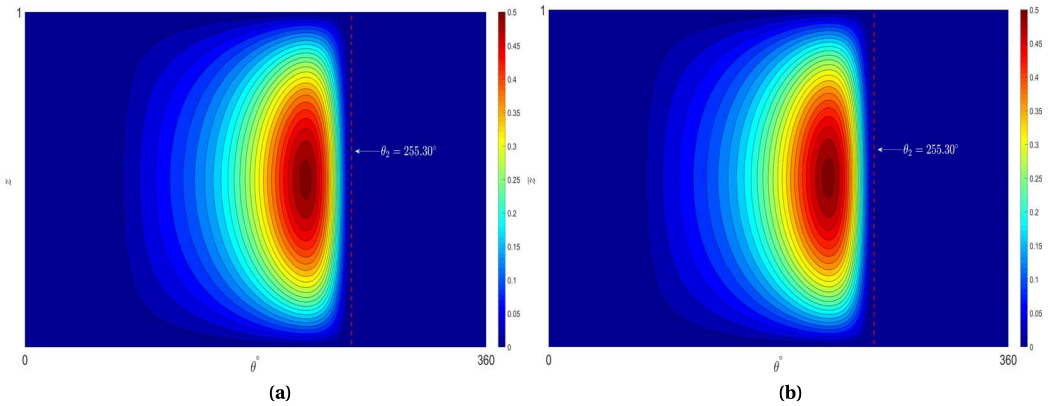

Figure 16. Dimensionless pressure fields versus axial and circumferential coordinates at $\alpha = 180°$ obtained by: (a) PGD and (b) FDM.

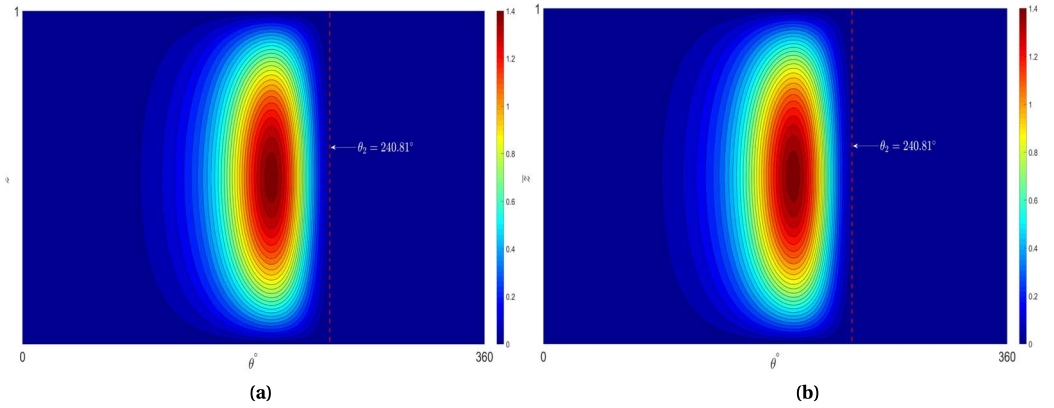

Figure 17. Dimensionless pressure distributions versus axial and circumferential coordinates at $\alpha = 270°$ obtained by: (a) PGD and (b) FDM.

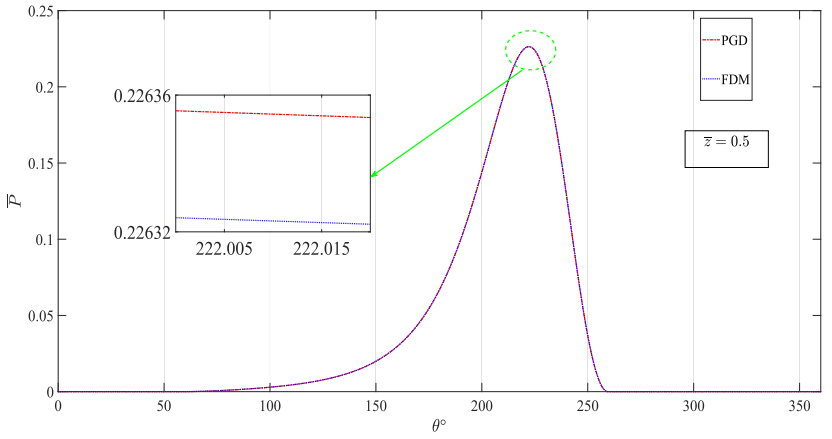

Figure 18. Dimensionless pressure distributions along the circumferential direction at mid-line ($\overline{z} = 0.5$) for $\alpha = 56°$.

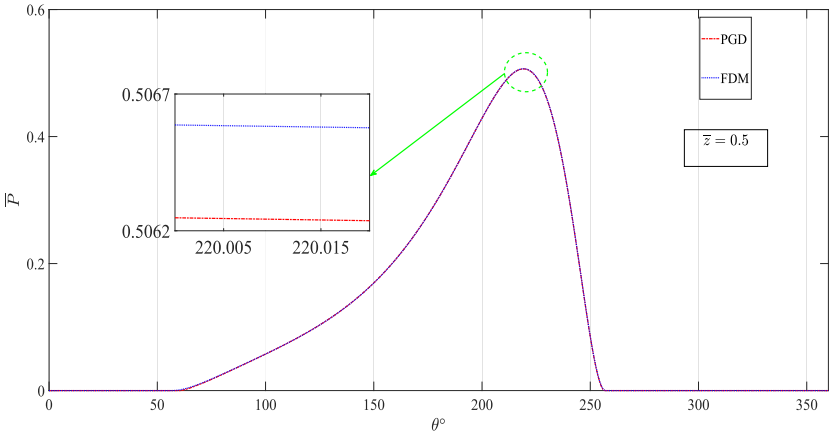

Figure 19. Dimensionless pressure distributions along the circumferential direction at mid-line ($\overline{z} = 0.5$) for $\alpha = 180°$.

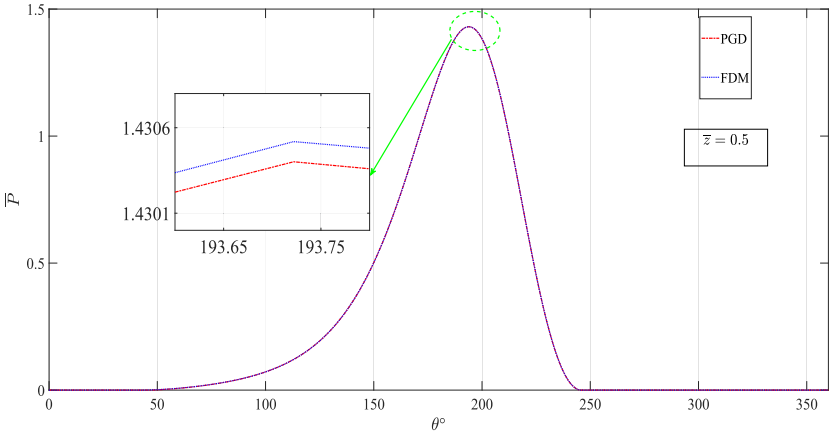

Figure 20. Dimensionless pressure distributions along the circumferential direction at mid-line ($\overline{z} = 0.5$) for $\alpha = 270°$.

Through these comparisons, it can seen that the pressure curves obtained by the PGD are very close to those of the FDM.

4.2.2. *Journal center orbits*

Figure 21 presents the trajectory of journal center during the load cycle obtained by the PGD and FDM. It is noted that, the results obtained by the two approaches are in very good correspondence.

4.2.3. *Sommerfeld and friction numbers*

Figure 22 shows the variation of Sommerfeld number as a function of the crank angle obtained by the PGD and the FDM. Through this comparison, it is clear that the number of Sommerfeld obtained by the PGD is very consistent with the results of the FDM.

The friction number is calculated during the load cycle using the PGD and the FDM and is illustrated in Figure 23. From this figure, it can be discerned that the friction number computed by the PGD agree with solution calculated by FDM.

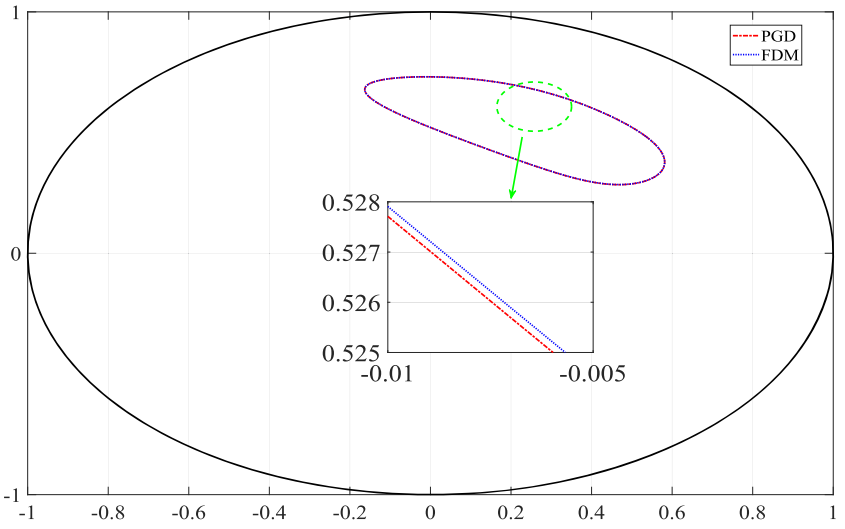

Figure 21. Journal center orbit over a load cycle for finite journal bearing.

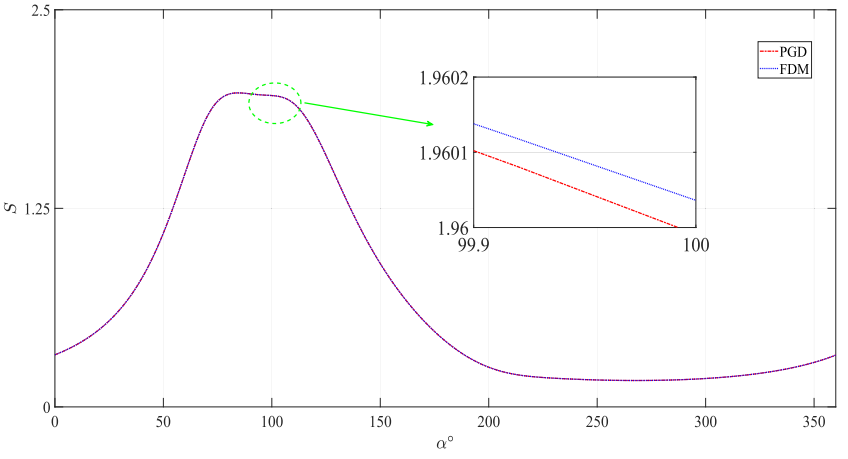

Figure 22. Variation of Sommerfeld number as a function of the crank angle.

4.2.4. *Mesh convergence study*

The convergence study is conducted using different sets of meshes. The obtained results are listed in Table 5 and plotted in Figure 24. It is noted that the convergence rate of the PGD is relatively better than that of the FDM for practically all sets nodes used.

4.2.5. *Computational time*

The computational time required to calculate the pressure distribution by the PGD and FDM techniques is represented in Figure 25 and Table 6. From this comparison, It can be seen that, the PGD approach is definitely more efficient (i.e. takes less time) than FDM. For example, in mesh size of $(1000 \times 101 \times 635)$, the PGD is more than one hundred and forty times faster than the FDM.

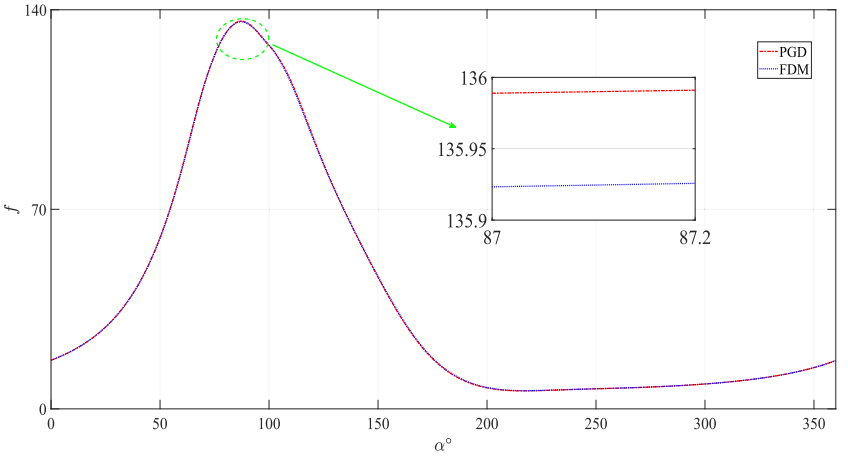

Figure 23. Variation of friction number as a function of the crank angle.

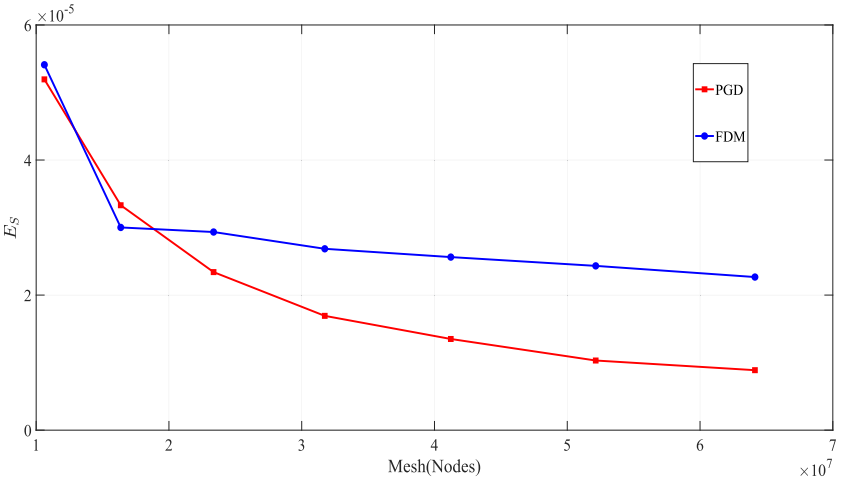

Figure 24. Error in Sommerfeld number computation for FJB using PGD and FDM.

Table 5. Error in Sommerfeld number computation for FJB using PGD and FDM

Mesh	Error E_S for ISJB	
	PGD	FDM
$1000 \times 41 \times 295$	5.1943×10^{-5}	5.4109×10^{-4}
$1000 \times 51 \times 321$	3.3303×10^{-5}	3.0015×10^{-5}
$1000 \times 61 \times 383$	2.3404×10^{-5}	2.9338×10^{-5}
$1000 \times 71 \times 447$	1.6923×10^{-5}	2.6854×10^{-5}
$1000 \times 81 \times 509$	1.7058×10^{-5}	2.5626×10^{-5}
$1000 \times 91 \times 573$	1.0310×10^{-5}	1.9325×10^{-5}
$1000 \times 101 \times 653$	8.8792×10^{-6}	1.2671×10^{-5}

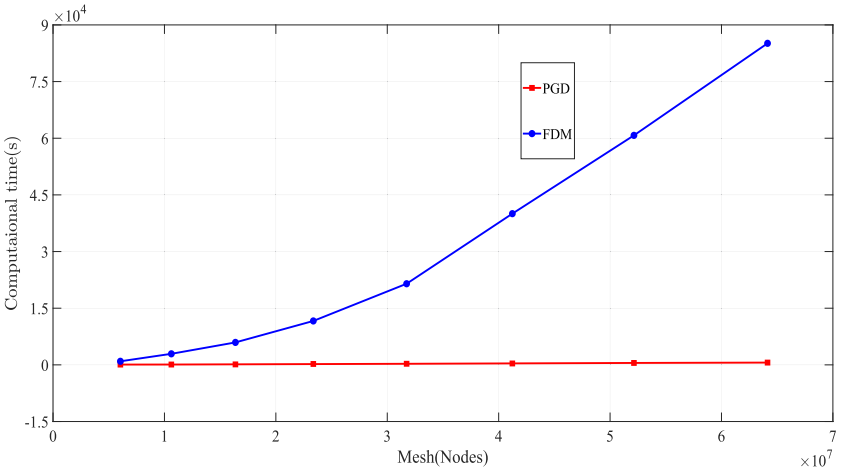

Figure 25. PGD versus FDM computational time for different number of nodes.

Table 6. PGD versus FDM, computational time for different number of nodes

Mesh	Computational time for FJB	
	PGD	FDM
$1000 \times 31 \times 195$	77.21	946.86
$1000 \times 41 \times 295$	89.67	2925.42
$1000 \times 51 \times 321$	123.74	5943.81
$1000 \times 61 \times 383$	239.41	11625.27
$1000 \times 71 \times 447$	290.49	21478.54
$1000 \times 81 \times 509$	367.71	40031.47
$1000 \times 91 \times 573$	508.57	60759.61
$1000 \times 101 \times 635$	603.43	85125.37

5. Conclusion

The study of hydrodynamic lubrication of dynamically loaded journal bearings is provided in this work using Proper Generalized Decomposition approach. The basic principle of the PGD method is to compute each term of the numerical approximation iteratively through the sum of specified functions products in lower dimensions. We have shown that when compared to the full discretized model, the PGD technique is able to solve the journal bearing transient problems of accuracy with significant low cost and much better convergence.

In terms of computational time, the results are absolutely impressive: the time consumed by the PGD remains relatively constant compared to the classical method, for example for a mesh size of ($N_\alpha = 1000$, $N_{\overline{z}} = 101$, $N_\theta = 653$) the PGD is one hundred times faster and one hundred and forty times faster than the classical method for a short journal bearing and finite journal bearing, respectively, with a better error order.

This study is the first step in addressing model order reduction in journal bearing hydrodynamic lubrication under dynamic load. Further research will be conducted to increase the order of complexity of this problem in order to solve the misaligned and textured journal bearings transient problems and adapting the PGD to the mass conservation model for the cavitation zone determination.

Nomenclature

e	Eccentricity (m)
c	Radial clearance (m)
μ	Dynamic viscosity (Pa·s)
ε	Relative eccentricity, $\varepsilon = \dfrac{e}{c}$
h	Film thickness (m)
D	Bearing diameter (m)
L	Bearing length (m)
$\overline{h}$	The dimensionless oil film thickness, $\overline{h} = \dfrac{h}{c}$
R	Bearing radius (m)
ω	shaft's angular velocity (rad/s)
x_1, y_1	Coordinate system fixed of the bushing (m)
x_2, y_2	Coordinate system changed with the line of centers (m)
θ	Absolute coordinate related to fixed system (rad)
θ'	Circumferential coordinate starting from the line of the centers of bearing and journal
t	Time (s)
α	Crank angle (rad), $\alpha = t$
ϕ	Attitude angle (rad)
$\dot{\varepsilon}$	Derivative of ε, $\dot{\varepsilon} = \dfrac{\mathrm{d}\varepsilon}{\mathrm{d}\alpha}$
$\dot{\phi}$	Derivative of ϕ, $\dot{\phi} = \dfrac{\mathrm{d}\phi}{\mathrm{d}\alpha}$
e_{x1}, e_{y1}	Components of eccentricity (m)
ε_{x1}, ε_{y1}	Components of relatives eccentricity
$\dot{\varepsilon}_{x1}$, $\dot{\varepsilon}_{y1}$	Derivative of ε_{x1} and ε_{y1}, respectively, $\dot{\varepsilon}_{x1} = \dfrac{\mathrm{d}\varepsilon_{x1}}{\mathrm{d}\alpha}$, $\dot{\varepsilon}_{y1} = \dfrac{\mathrm{d}\varepsilon_{y1}}{\mathrm{d}\alpha}$
$\ddot{\varepsilon}_{x1}$, $\ddot{\varepsilon}_{y1}$	Derivative of $\dot{\varepsilon}_{x1}$ and $\dot{\varepsilon}_{y1}$, respectively, $\ddot{\varepsilon}_{x1} = \dfrac{\mathrm{d}\dot{\varepsilon}_{x1}}{\mathrm{d}\alpha}$, $\ddot{\varepsilon}_{y1} = \dfrac{\mathrm{d}\dot{\varepsilon}_{y1}}{\mathrm{d}\alpha}$
P	Lubricant pressure (Pa)
$\overline{P}$	Dimensionless Lubricant pressure, $\overline{P} = \dfrac{Pc^2}{\mu R^2}$
$\overline{F}$	The dimensionless fluid film force
$\overline{F}_{x1}$, $\overline{F}_{y1}$	The components of the dimensionless fluid film force
W	The dynamic applied load, (N)
$\overline{W}$	The dimensionless externally applied load, $\overline{W} = \dfrac{Wc^2}{L\mu R^3}$
$\overline{W}_{x1}$, $\overline{W}_{y1}$	The components of the dimensionless externally applied load
U	Shaft speed (m/s)
S	Sommerfeld number
$\overline{F}_t$	Dimensionless friction force
M	Mass of journal, (kg)
$\overline{M}$	Dimensionless mass, $\overline{M} = \dfrac{Mc^2}{L\mu R^3}$
f	Friction number
τ_{xy}	Shearing stresses (Pa)

Conflicts of interest

Authors have no conflict of interest to declare.

Appendix A.

To translate from (x_1, y_1) to (x_2, y_2), the following parameters are used;

$$\begin{cases} \varepsilon = \sqrt{\varepsilon_{x1}^2 + \varepsilon_{y1}^2} \\ \phi = \arcsin\left(\dfrac{\varepsilon_{y1}}{\varepsilon}\right) \\ \overline{h} = 1 + \varepsilon\cos(\theta') \\ \dot{\varepsilon} = \dot{\varepsilon}_{y1}\sin(\phi) + \dot{\varepsilon}_{x1}\cos(\phi) \\ \dot{\phi} = \dfrac{1}{\varepsilon}\left(\dot{\varepsilon}_{y1}\cos(\phi) - \dot{\varepsilon}_{x1}\sin(\phi)\right). \end{cases} \tag{A.1}$$

By applying the boundary conditions on (2.23), the location of the starting of full film zone (θ_1') and the cavitation area (θ_2') are obtained by:

$$(2\,\varepsilon\,\dot{\phi} - \varepsilon)\,\sin(\theta') + 2\,\dot{\varepsilon}\,\cos(\theta') = 0. \tag{A.2}$$

To calculate the fluid film forces, the following equations are used:

$$\begin{cases} \overline{F}_{x2} = -\displaystyle\int_0^1 \int_{\theta_1'}^{\theta_2'} \overline{P}\cos(\theta')\,\mathrm{d}\theta'\,\mathrm{d}\overline{z} \\ \overline{F}_{y2} = -\displaystyle\int_0^1 \int_{\theta_1'}^{\theta_2'} \overline{P}\sin(\theta')\,\mathrm{d}\theta'\,\mathrm{d}\overline{z}. \end{cases} \tag{A.3}$$

To solve integral on (A.3), the Sommerfeld change of variables [34] are employed as follow:

$$\begin{cases} 1 + \varepsilon\cos(\theta') = \dfrac{1-\varepsilon^2}{1-\varepsilon\cos(\psi)} \\ \cos(\theta') = \dfrac{-\varepsilon + \cos(\psi)}{1-\varepsilon\cos(\psi)} \\ \sin(\theta') = \dfrac{(1-\varepsilon^2)^{\frac{1}{2}}\sin(\psi)}{1-\varepsilon\cos(\psi)} \\ \mathrm{d}\theta' = \dfrac{(1-\varepsilon^2)^{\frac{1}{2}}}{1-\varepsilon\cos(\psi)}\,\mathrm{d}\psi. \end{cases} \tag{A.4}$$

By using (A.4) and solving integrals (see Appendix C), the (A.3) becomes:

$$\begin{cases} \overline{F}_{x2} = \dfrac{-1}{2\,\eta^2}\left(A(\psi_2) - A(\psi_1)\right) \\ \overline{F}_{y2} = \dfrac{-1}{2\,\eta^2}\left(B(\psi_2) - B(\psi_1)\right) \end{cases} \tag{A.5}$$

where:

$$\begin{cases} A(\psi) = 2\dot{\varepsilon}\,\dfrac{1}{(1-\varepsilon^2)^{\frac{5}{2}}}\left(\psi\left(2\varepsilon^2+\dfrac{1}{2}\right)+\dfrac{\sin(2\psi)}{4}-2\varepsilon\sin(\psi)\right)+(2\varepsilon\dot{\phi}-\varepsilon)\,\dfrac{1}{2(1-\varepsilon^2)^{\frac{3}{2}}}(\psi-\sin(\psi)\cos(\psi)) \\ B(\psi) = 2\dot{\varepsilon}\,\dfrac{1}{2(1-\varepsilon^2)^{\frac{3}{2}}}(\psi-\sin(\psi)\cos(\psi))+(2\varepsilon\dot{\phi}-\varepsilon)\,\dfrac{1}{(1-\varepsilon^2)^{\frac{5}{2}}}\left(\psi\left(2\varepsilon^2+\dfrac{1}{2}\right)+\dfrac{\sin(2\psi)}{4}-2\varepsilon\sin(\psi)\right) \\ \psi_i = 2\,\mathrm{arctg}\left(\left(\sqrt{\dfrac{1-\varepsilon}{1+\varepsilon}}\right)\mathrm{tg}\left(\dfrac{\theta'_i}{2}\right)\right). \end{cases} \tag{A.6}$$

To return to the x_1, y_1 coordinates, the following changes are used:

$$\begin{cases} \overline{F}_{x1} = -\overline{F}_{x2}\sin(\phi)-\overline{F}_{y2}\cos(\phi) \\ \overline{F}_{y1} = -\overline{F}_{x2}\cos(\phi)+\overline{F}_{y2}\sin(\phi). \end{cases} \tag{A.7}$$

Appendix B.

Integrating (2.25) once with respect to θ', one arrives at:

$$\frac{\partial\overline{P}}{\partial\theta'} = 6\left[(1-2\dot{\phi})\,\varepsilon\,\frac{\cos(\theta')}{(1+\varepsilon\cos(\theta'))^3}+2\dot{\varepsilon}\,\frac{\sin(\theta')}{(1+\varepsilon\cos(\theta'))^3}+\frac{C_1}{(1+\varepsilon\cos(\theta'))^3}\right] \tag{B.1}$$

where $C_1 \neq C_1(\theta')$.

C_1 is obtained by applying the (2.12) on (B.1), So:

$$C_1 = -(1-2\dot{\phi})\,\varepsilon\cos(\theta'_2)-2\dot{\varepsilon}\sin(\theta'_2). \tag{B.2}$$

Integrating (B.1) with C_1 given in (B.2), the following expression is obtained:

$$\begin{aligned}\overline{P} = {} & \frac{6}{(1-\varepsilon^2)^{1.5}}\left[(1-2\dot{\phi})\,(1-\varepsilon^2)^2\,(\psi-\varepsilon\sin(\psi))+\dot{\varepsilon}\,\frac{(1-\varepsilon\cos(\psi))^2}{\varepsilon}\right. \\ & \left.-\frac{(1-2\dot{\phi})\,(1-\varepsilon^2)^{0.5}+2\dot{\varepsilon}\sin(\psi_2)}{1-\varepsilon\cos(\psi_2)}\left(\psi+\frac{\varepsilon^2}{2}\psi-2\varepsilon\sin(\psi)-\frac{\varepsilon^2\sin(2\psi)}{4}\right)+C_2\right].\end{aligned} \tag{B.3}$$

With $C_2 \neq C_2(\theta')$, applying the (2.9) on (B.3), get:

$$\begin{aligned}C_2 = {} & -(1-2\dot{\phi})\,(1-\varepsilon^2)^2\,(\psi_0-\varepsilon\sin(\psi_0))-\dot{\varepsilon}\,\frac{(1-\varepsilon\cos(\psi_0))^2}{\varepsilon} \\ & +\frac{(1-2\dot{\phi})\,(1-\varepsilon^2)^{0.5}+2\dot{\varepsilon}\sin(\psi_2)}{1-\varepsilon\cos(\psi_2)}\left(\psi_0+\frac{\varepsilon^2}{2}\psi_0-2\varepsilon\sin(\psi_0)-\frac{\varepsilon^2\sin(2\psi_0)}{4}\right)\end{aligned} \tag{B.4}$$

where ψ_0 corresponds to $\theta'_0 = -\phi$, which defines the oil inlet position.

Because the oil film pressure only exists in the range of $\theta'_1 \le \theta' \le \theta'_2$, the dynamic pressure given by (2.26) is true for $\psi_1 \le \psi \le \psi_2$. The oil film pressure is nil outside of this range.

Using the boundary conditions specified by (2.9) and (2.10) to predict the constants in (2.26). The starting film zone position ψ_1 and the starting location of cavitation ψ_2 can be determined by the following equations:

$$\begin{aligned}&(1-2\dot{\phi})\,\varepsilon\,(1-\varepsilon^2)^{0.5}\,[(2+\varepsilon\cos(\psi_2))\,(\sin(\psi_2)-\sin(\psi_0))-\varepsilon\sin(\psi_0)\,(\cos(\psi_2)-\cos(\psi_0)) \\ &\quad+(2\cos(\psi_2)+\varepsilon)\,(\psi_0-\psi_2)]+2\dot{\varepsilon}\,[(2\cos(\psi_0)-2\cos(\psi_2)+\varepsilon\sin^2(\psi_0))\,(1-\varepsilon\cos(\psi_2)) \\ &\quad-\varepsilon\sin(\psi_0)\sin(\psi_2)\,(4-\varepsilon\cos(\psi_0))-(2+\varepsilon^2)\sin(\psi_2)\,(\psi_2-\psi_0)+3\varepsilon\sin^2(\psi_2)]=0\end{aligned} \tag{B.5}$$

$$\begin{aligned}&(1-2\dot{\phi})\,\varepsilon\,(1-\varepsilon^2)^{0.5}\,[(2+\varepsilon\cos(\psi_1))\,(\sin(\psi_1)-\sin(\psi_0))-\varepsilon\sin(\psi_0)\,(\cos(\psi_2)-\cos(\psi_0)) \\ &\quad+(2\cos(\psi_1)+\varepsilon)\,(\psi_0-\psi_1)]+2\dot{\varepsilon}\,[(2\cos(\psi_0)-2\cos(\psi_1)+\varepsilon\sin^2(\psi_0))\,(1-\varepsilon\cos(\psi_1)) \\ &\quad-\varepsilon\sin(\psi_0)\sin(\psi_1)\,(4-\varepsilon\cos(\psi_0))-(2+\varepsilon^2)\sin(\psi_2)\,(\psi_1-\psi_0)+3\varepsilon\sin^2(\psi_1)]=0.\end{aligned} \tag{B.6}$$

By using (A.4) in Appendix A and solving the integrals (see Appendix C), the dimensionless radial and tangential fluid force components are given by:

$$F_{x2} = -3\left[\frac{(1-2\dot{\phi})\,\varepsilon\,(\cos(\psi_2)-\cos(\psi_1))^2}{(1-\varepsilon^2)\,(1-\varepsilon\cos(\psi_2))} + 2\,\dot{\varepsilon} \times \frac{(\psi_2-\psi_1+\sin(\psi_1)\cos(\psi_1))\,(1-\varepsilon\cos(\psi_2))}{(1-\varepsilon^2)^{1.5}\,(1-\varepsilon\cos(\psi_2))} \times \frac{(\varepsilon\cos^2(\psi_1)-2\cos(\psi_1)+\cos(\psi_2))\sin(\psi_2)}{(1-\varepsilon^2)^{1.5}\,(1-\varepsilon\cos(\psi_2))}\right] \tag{B.7}$$

$$\begin{aligned} F_{y2} = 3\Bigg\{ & \frac{(1-2\dot{\phi})\,\varepsilon}{(1-\varepsilon^2)^{1.5}(1-\varepsilon\cos(\psi_2))}\left[(1+2\varepsilon\cos(\psi))\,(\psi_2-\psi_1)-2\,(\varepsilon+\cos(\psi_2))\,(\sin(\psi_2)-\sin(\psi_1))\right. \\ & \left.+\,(\sin(\psi_2)\cos(\psi_2)-\sin(\psi_1)\cos(\psi_1))\right]+\frac{2\,\dot{\varepsilon}}{(1-\varepsilon^2)^{1.5}\,(1-\varepsilon\cos(\psi_2))}\left[2\,\varepsilon\,(\cos(\psi_2)-\varepsilon)\right. \\ & -(2\,\varepsilon\cos(\psi_1)+\sin^2(\psi_1))\,(1-\varepsilon\cos(\psi_2))-\sin^2(\psi_2) \\ & \left.+\,3\,\varepsilon\sin(\psi_2)\,(\psi_2-\psi_1)+(2\,\varepsilon^2+2-\varepsilon\cos(\psi_1))\sin(\psi_1)\sin(\psi_2)\right]\Bigg\}. \end{aligned} \tag{B.8}$$

Equation (A.7) in Appendix A can be used to return to the x_1, y_1 coordinates.

Appendix C.

By using (A.4) to calculate the integral of the following form $J_l^{nm} = \int(\sin^m(\theta')\cos^n(\theta')/(1+\varepsilon\cos(\theta'))^l)\,\mathrm{d}\theta'$, the following results are obtained:

$$J_3^{00} = \frac{1}{(1-\varepsilon^2)^{2.5}}\left(\psi+\frac{\varepsilon^2}{2}\,\psi-2\,\varepsilon\sin(\psi)+\frac{\varepsilon^2\sin(2\,\psi)}{4}\right) \tag{C.1}$$

$$J_3^{10} = \frac{(1-\varepsilon\cos(\psi))^2}{\varepsilon\,(1-\varepsilon^2)^2} \tag{C.2}$$

$$J_3^{01} = \frac{-3\,\varepsilon\,\psi+2\,(1+\varepsilon^2)\sin(\psi)-\varepsilon\sin(\psi)\cos(\psi)}{2\,(1-\varepsilon^2)^{2.5}} \tag{C.3}$$

$$J_3^{11} = \frac{(1-2\,\varepsilon^2+\varepsilon\cos(\psi))\,(1-\varepsilon\cos(\psi))}{2\,\varepsilon^2\,(1-\varepsilon^2)^2} \tag{C.4}$$

$$J_3^{20} = \frac{\psi-\sin(\psi)\cos(\psi)}{2\,(1-\varepsilon^2)^{1.5}} \tag{C.5}$$

$$J_3^{02} = \frac{(1+2\,\varepsilon^2)\,\psi-4\,\varepsilon\sin(\psi)+\sin(\psi)\cos(\psi)}{2\,(1-\varepsilon^2)^{1.5}}. \tag{C.6}$$

References

[1] O. Reynolds, "IV. On the theory of lubrication and its application to Mr. Beauchamp tower's experiments, including an experimental determination of the viscosity of olive oil", *Philos. Trans. R. Soc. Lond.* **177** (1886), p. 157-234.

[2] N. Petrov, "Friction in machines and the effect of the lubricant", *Inzh. Zh., St-Peterb.* **1** (1883), p. 71-140.

[3] B. Tower, "First report on friction experiments", *Proc. Inst. Mech. Eng.* **34** (1883), no. 1, p. 632-659.

[4] J. Wang, M. Khonsari, "Effects of oil inlet pressure and inlet position of axially grooved infinitely long journal bearings. Part I: Analytical solutions and static performance", *Tribol. Int.* **41** (2008), no. 2, p. 119-131.

[5] R.-Z. Gong, D.-Y. Li, H.-J. Wang, L. Han, D.-Q. Qin, "Analytical solution of Reynolds equation under dynamic conditions", *Proc. Inst. Mech. Eng. J: J. Eng. Tribol.* **230** (2016), no. 4, p. 416-427.

[6] H. Hirani, K. Athre, S. Biswas, "Dynamically loaded finite length journal bearings: analytical method of solution", *J. Tribol.* **121** (1999), no. 4, p. 844-852.

[7] R. Kirk, E. Gunter, "Short bearing analysis applied to rotor dynamics—Part I: Theory", *J. Lubr. Technol.* **98** (1976), p. 47-56.

[8] T. Han, R. Paranjpe, "A finite volume analysis of the thermohydrodynamic performance of finite journal bearings", *J. Tribol.* **112** (1990), no. 3, p. 557-565.
[9] R. Paranjpe, "Analysis of non-Newtonian effects in dynamically loaded finite journal bearings including mass conserving cavitation", *J. Tribol.* **114** (1992), no. 4, p. 736-744.
[10] R. S. Paranjpe, T. Han, "A study of the thermohydrodynamic performance of steadily loaded journal bearings", *Tribol. Trans.* **37** (1994), no. 4, p. 679-690.
[11] P. K. Goenka, "Dynamically loaded journal bearings: finite element method analysis", *J. Tribol.* **106** (1984), no. 4, p. 429-437.
[12] R. S. Paranjpe, P. K. Goenka, "Analysis of crankshaft bearings using a mass conserving algorithm", *Tribol. Trans.* **33** (1990), no. 3, p. 333-344.
[13] B. Vincent, P. Maspeyrot, J. Frene, "Cavitation in dynamically loaded journal bearings using mobility method", *Wear* **193** (1996), no. 2, p. 155-162.
[14] X.-L. Wang, K.-Q. Zhu, S.-Z. Wen, "On the performance of dynamically loaded journal bearings lubricated with couple stress fluids", *Tribol. Int.* **35** (2002), no. 3, p. 185-191.
[15] X.-L. Wang, K.-Q. Zhu, "A study of the lubricating effectiveness of micropolar fluids in a dynamically loaded journal bearing (T1516", *Tribol. Int.* **37** (2004), no. 6, p. 481-490.
[16] C. Allery, S. Guérin, A. Hamdouni, A. Sakout, "Experimental and numerical POD study of the Coanda effect used to reduce self-sustained tones", *Mech. Res. Commun.* **31** (2004), no. 1, p. 105-120.
[17] C. Allery, C. Beghein, A. Hamdouni, "On investigation of particle dispersion by a POD approach", *Int. Appl. Mech.* **44** (2008), no. 1, p. 110-119.
[18] J. A. Atwell, B. B. King, "Proper orthogonal decomposition for reduced basis feedback controllers for parabolic equations", *Math. Comput. Model.* **33** (2001), no. 1-3, p. 1-19.
[19] N. Akkari, A. Hamdouni, E. Liberge, M. Jazar, "A mathematical and numerical study of the sensitivity of a reduced order model by POD (ROM–POD), for a 2D incompressible fluid flow", *J. Comput. Appl. Math.* **270** (2014), p. 522-530.
[20] M. Krasnyk, M. Mangold, A. Kienle, "Reduction procedure for parametrized fluid dynamics problems based on proper orthogonal decomposition and calibration", *Chem. Eng. Sci.* **65** (2010), no. 23, p. 6238-6246.
[21] A. Ammar, B. Mokdad, F. Chinesta, R. Keunings, "A new family of solvers for some classes of multidimensional partial differential equations encountered in kinetic theory modeling of complex fluids", *J. Non-Newtonian Fluid Mech.* **139** (2006), no. 3, p. 153-176.
[22] F. Chinesta, A. Ammar, E. Cueto, "On the use of proper generalized decompositions for solving the multidimensional chemical master equation", *Eur. J. Comput. Mech./Revue Européenne de Mécanique Numérique* **19** (2010), no. 1-3, p. 53-64.
[23] A. Ammar, P. Joyot, "The nanometric and micrometric scales of the structure and mechanics of materials revisited: an introduction to the challenges of fully deterministic numerical descriptions", *Int. J. Multiscale Comput. Eng.* **6** (2008), no. 3, p. 191-213.
[24] A. Dumon, C. Allery, A. Ammar, "Proper general decomposition (PGD) for the resolution of Navier–Stokes equations", *J. Comput. Phys.* **230** (2011), no. 4, p. 1387-1407.
[25] M. S. Aghighi, A. Ammar, C. Metivier, M. Normandin, F. Chinesta, "Non-incremental transient solution of the Rayleigh–Bénard convection model by using the PGD", *J. Non-Newtonian Fluid Mech.* **200** (2013), p. 65-78.
[26] A. Dumon, C. Allery, A. Ammar, "Proper generalized decomposition method for incompressible Navier–Stokes equations with a spectral discretization", *Appl. Math. Comput.* **219** (2013), no. 15, p. 8145-8162.
[27] C. Leblond, C. Allery, "A priori space–time separated representation for the reduced order modeling of low Reynolds number flows", *Comput. Methods Appl. Mech. Eng.* **274** (2014), p. 264-288.
[28] L. Tamellini, O. Le Maitre, A. Nouy, "Model reduction based on proper generalized decomposition for the stochastic steady incompressible Navier–Stokes equations", *SIAM J. Sci. Comput.* **36** (2014), no. 3, p. A1089-A1117.
[29] C. Le-Quoc, L. A. Le, V. Ho-Huu, P. Huynh, T. Nguyen-Thoi, "An immersed boundary proper generalized decomposition (IB-PGD) for fluid–structure interaction problems", *Int. J. Comput. Methods* **15** (2018), no. 06, article no. 1850045.
[30] B. Cherabi, A. Hamrani, I. Belaidi, S. Khelladi, F. Bakir, "An efficient reduced-order method with PGD for solving journal bearing hydrodynamic lubrication problems", *C. R. Méc.* **344** (2016), no. 10, p. 689-714.
[31] J. Frene, D. Nicolas, B. Degueurce, D. Berthe, M. Godet, *Hydrodynamic Lubrication: Bearings and Thrust Bearings*, Elsevier, Amsterdam, 1997.
[32] A. Michell, "Progress in fluid film lubrication", *Trans. ASME* **51** (1929), no. 2, p. 153-163.
[33] G. B. DuBois, F. W. Ocvirk, "Analytical derivation and experimental evaluation of short-bearing approximation for full journal bearing", Tech. report, 1953.
[34] M. Born, "Arnold Johannes Wilhelm Sommerfeld 1868–1951", *Obituary Notices of Fellows R. Soc.* **8** (1952), p. 274-296.